Nonlinear optical probing and control of magnetic and electronic quantum geometry

Gregory A. Fiete
Northeastern University

Center for Dynamics and Control of Materials: an NSF MRSEC

Outline

- Motivation
  - Diversity of knobs for material control/probing
  - Experimental examples of driven materials
- Tuning the effective twist angle using a Floquet drive.
- Non-linear phononics—modifying magnetism and band topology (CrI_3 and $MnBi_2Te_4$).
- Nonlinear optical response (shift & injection currents) of Weyl systems as a probe of quantum geometry.
- Nonlinear optical response of superconductors as a probe of topology.
- Nonlinear optical response of ABC rhombohedral graphene as a probe of quantum geometry.

Laser Parameters for Driven Materials

- Parameters that can be controlled
  - Polarization (linear vs. circular)
  - Frequency (selectively couple to electrons or phonons)
  - Intensity (fluence, time integrated flux of laser)
  - Angle of incidence relative to material orientation
  - Pulse shaping (used in quantum chemistry)
  - Multiple drive lasers (could produce a "response on top of a response")

Experimental Realization of Floquet (time-periodic) Systems

- **Time-resolved ARPES: Nuh Gedik Group, MIT**

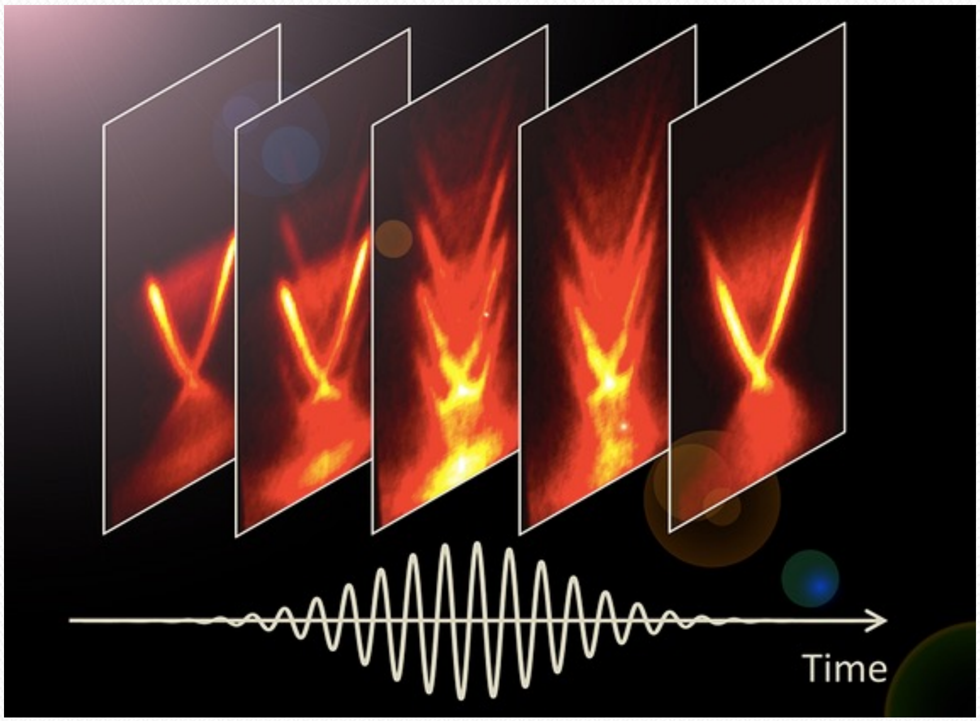

Surface states of Bi_2Se_3

Floquet states appear and go as periodic drive is present and then absent. (Subgap drive.)

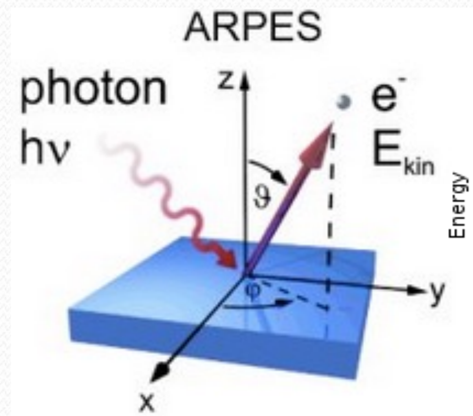

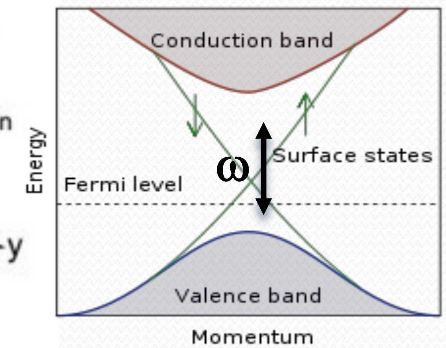

Wang, Steinberg, Jarillo-Herrero, and Gedik *Science* (2013)
Mahmood, Chan, Alpichshev, Gardner, Lee, Lee, and Gedik *Nat. Phys*. (2016)

Light induced anomalous Hall effect in graphene

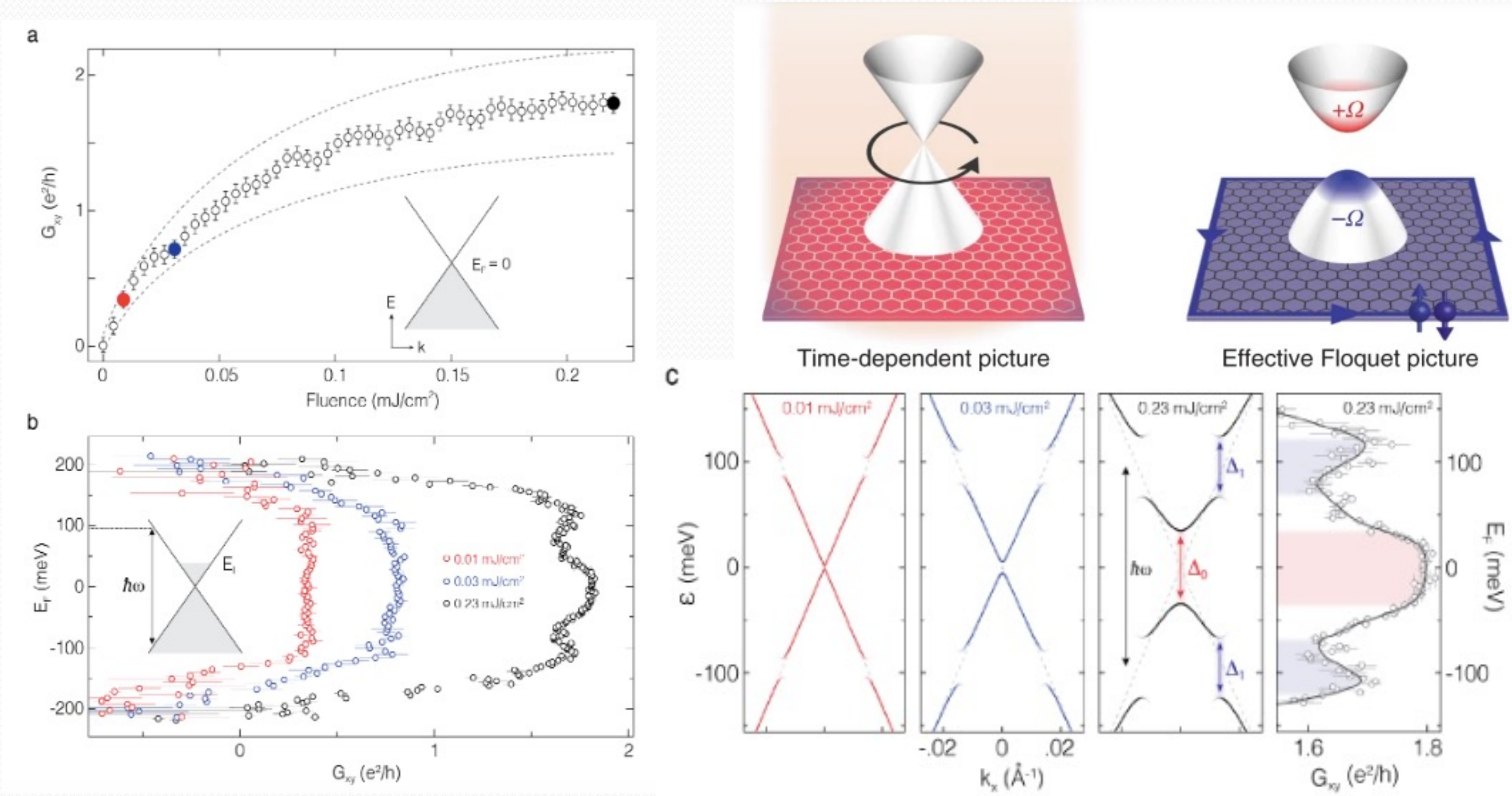

J. W. McIver, B. Schulte, F.-U. Stein, T. Matsuyama, G. Jotzu, G. Meier and A. Cavalleri, *Nature Physics* **16**, 38 (2020).

Hamiltonian of twisted bilayer graphene

$$H_{\mathbf{k}}(\mathbf{x}) = \begin{pmatrix} h(-\theta/2, \mathbf{k}-\kappa_-) & T(\mathbf{x}) \\ T^\dagger(\mathbf{x}) & h(\theta/2, \mathbf{k}-\kappa_+) \end{pmatrix}$$

$$h(\theta, \mathbf{k}) = \gamma \begin{pmatrix} 0 & f(R(\theta)\mathbf{k}) \\ f^*(R(\theta)\mathbf{k}) & 0 \end{pmatrix}$$

$$T(\mathbf{x}) = \sum_{i=-1}^{1} e^{-i\mathbf{b}_i \mathbf{x}} T_i,$$

$$T_i = w_0 \mathbb{1}_2 + w_1 \left(\cos\left(\frac{2\pi n}{3}\right)\sigma_1 + \sin\left(\frac{2\pi n}{3}\right)\sigma_2 \right)$$

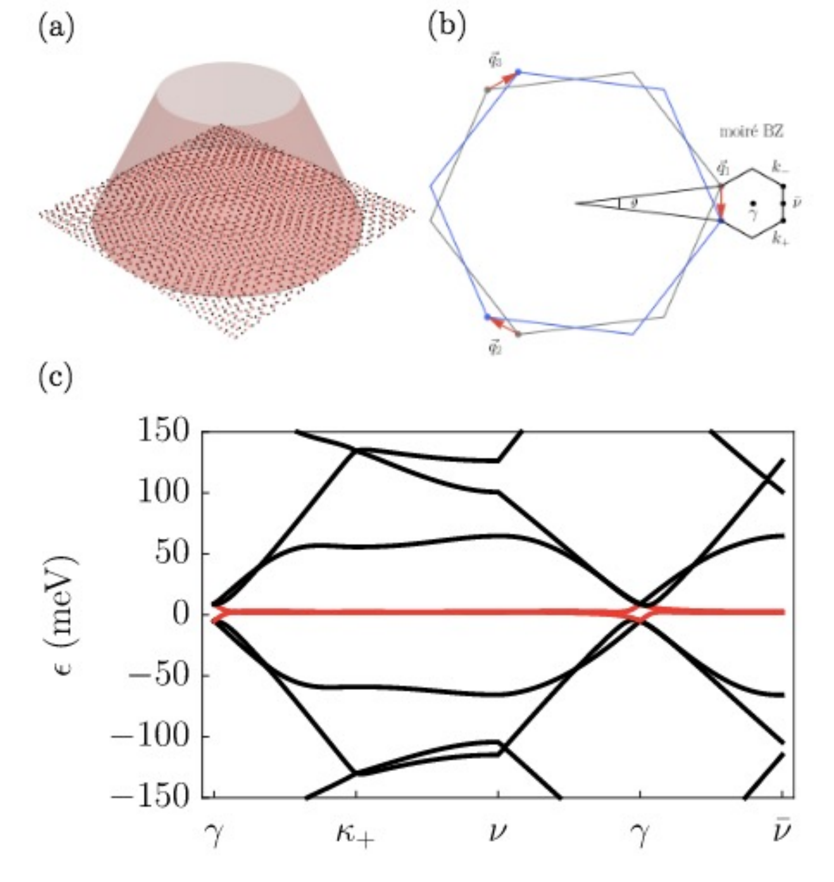

M. Vogl, M. Rodriguez-Vega, GAF *Phys. Rev. B* 101, 235411 (2020).

Direct control of the interlayer twist angle: Creation of longitudinal vector potential

$$t_{ij} \to t_{ij} \exp\left(-i \int_{\mathbf{r}_i}^{\mathbf{r}_j} \mathbf{A} \cdot d\mathbf{l}\right)$$

$$\mathbf{A} = \hat{z} A \sin(m\pi x/a) \sin(n\pi y/b) \mathrm{Re}(e^{-ik_z z - i\Omega t})$$

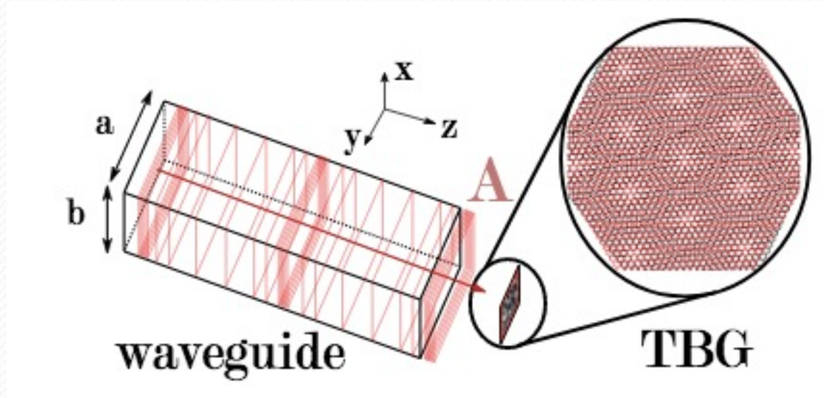

$$H = \begin{pmatrix} h(-\theta/2, \mathbf{k} - \kappa_-) & T(\mathbf{x}) \\ T^\dagger(\mathbf{x}) & h(\theta/2, \mathbf{k} - \kappa_+) \end{pmatrix}$$

$$T_n = w_0 \mathbb{1}_2 + w_1 \left(\cos\left(\frac{2\pi n}{3}\right)\sigma_1 + \sin\left(\frac{2\pi n}{3}\right)\sigma_2\right)$$

$$w_1 \to w_1 e^{-i a_{AB} A \cos(\Omega t)}$$

$$w_0 \to w_0 e^{-i a_{AA} A \cos(\Omega t)}$$

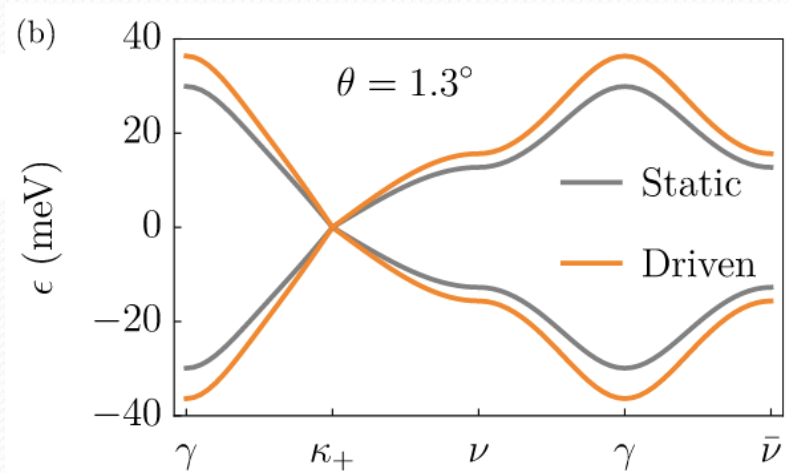

M. Vogl, M. Rodriguez-Vega, GAF *Phys. Rev. B* 101, 241408(R) (2020).

Direct control of the effective interlayer twist angle: Increasing or decreasing

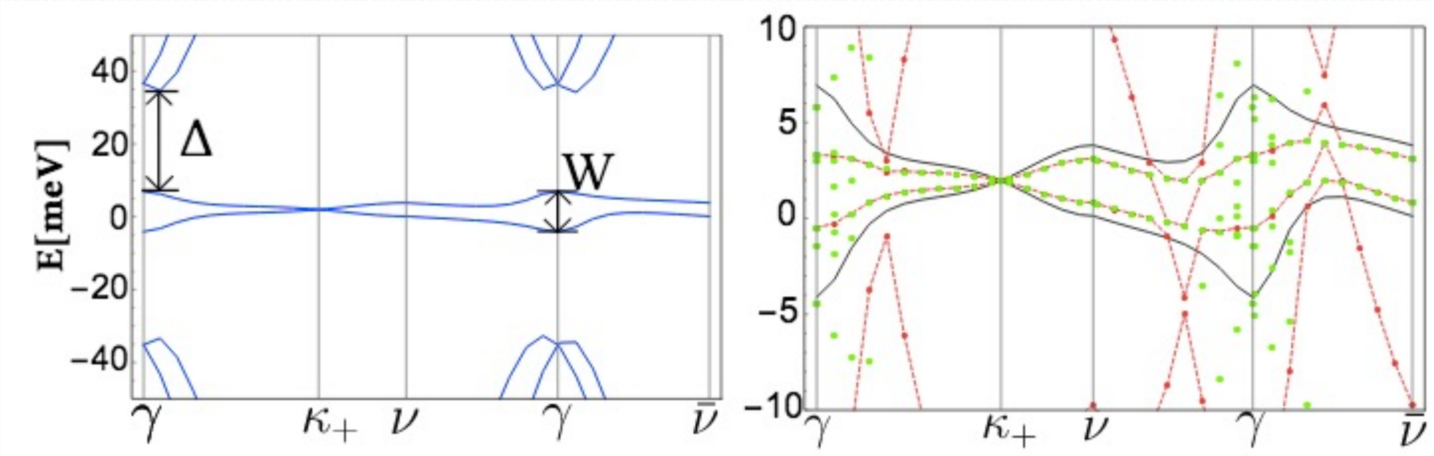

Magic angles tuned by light *in situ*! Increased or Decreased.

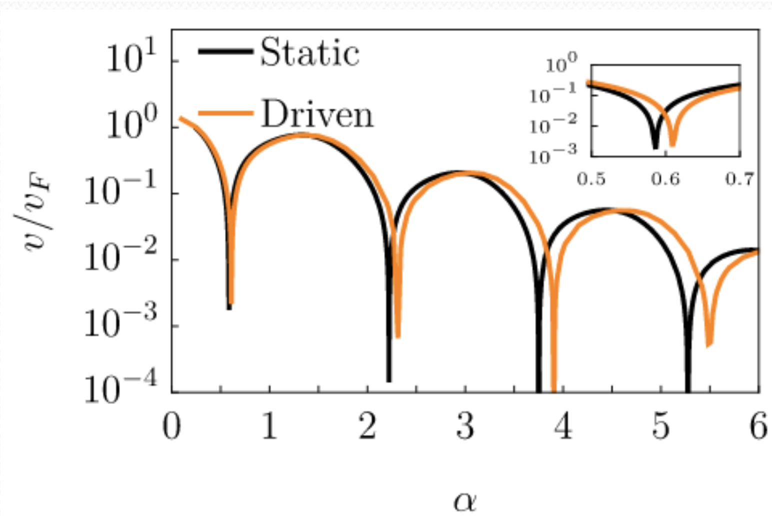

$$\theta_n = \frac{w_1 J_0\left(|a_{AB}A|\right)}{v_F k_D \alpha_n}$$

High frequency limit

M. Vogl, M. Rodriguez-Vega, GAF *Phys. Rev. B* 101, 241408(R) (2020).

Experimental results for bilayer CrI_3

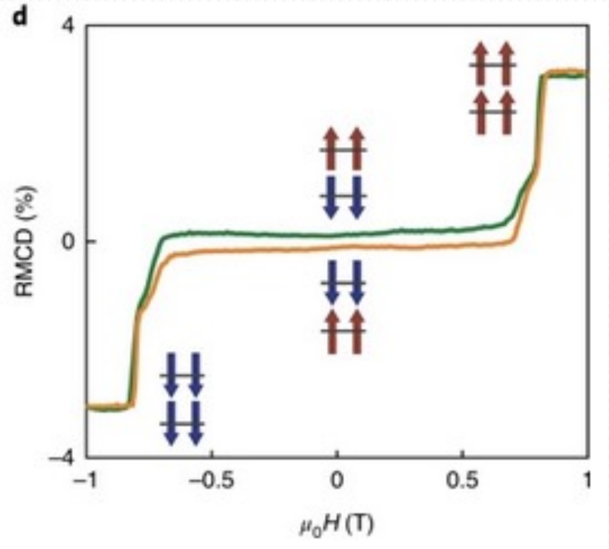

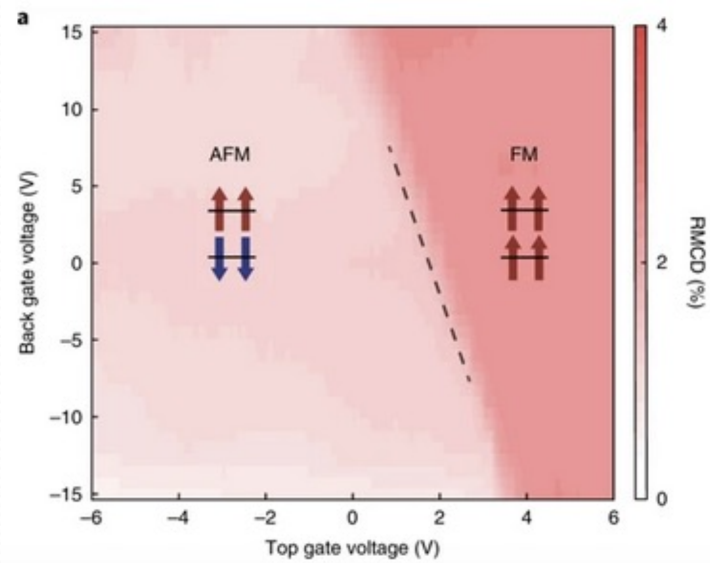

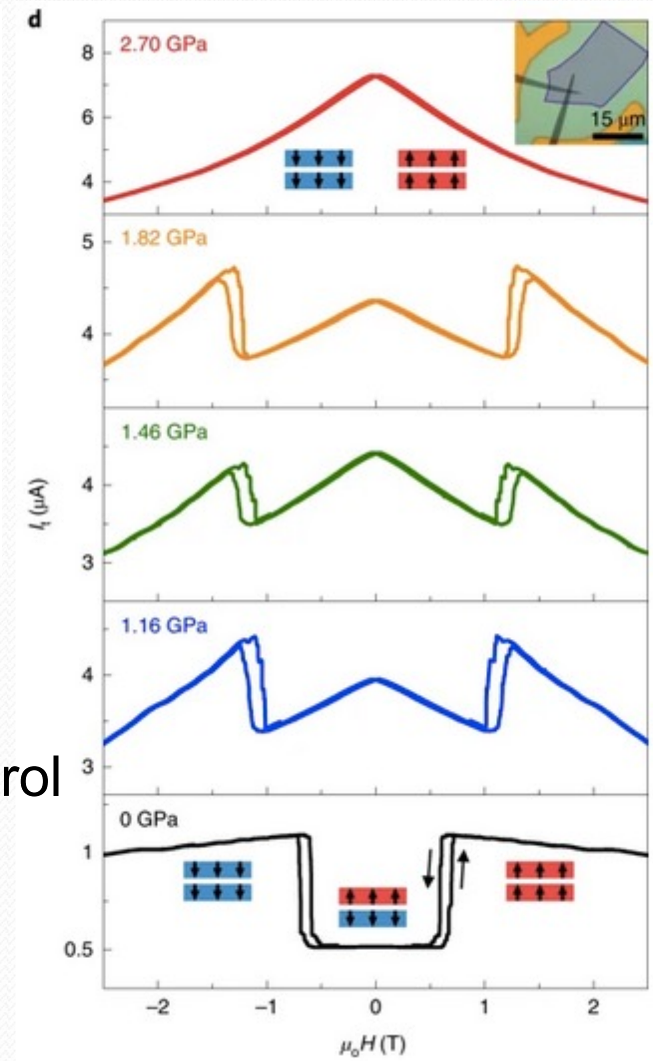

Magnetic field control of magnetism

Bevin Huang, …., Xiaodong Xu, *Nat. Nano*. **13**, 544 (2018)

Electric field control of magnetism

Pressure control of magnetism

- Can we create an analogous response with a laser drive?

Tiancheng Song, …, Xiaodong Xu, Nat. Mat. 18, 1298 (2019)

Non-linear phononics

- Selectively excite infrared active modes to create transient lattice distortion through nonlinearly coupled Raman modes → temporarily shifts equilibrium ion positions which modifies electronic properties.

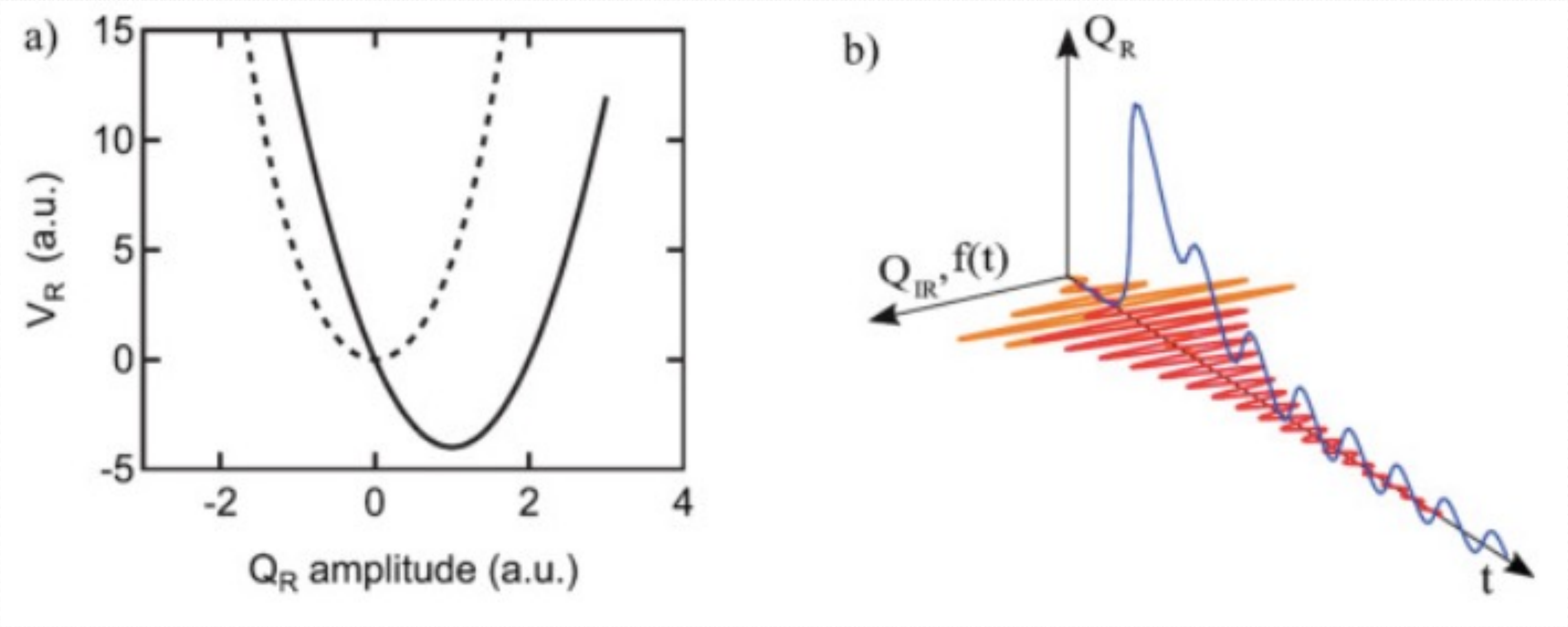

Mankowsky, Forst, and Cavalleri, *Rep. Prog. Phys*. **79**, 064503 (2016)

Phonon mediated dimensional crossover in CrI_3

- <u>Idea</u>: modulate interlayer exchange coupling via nonlinear phonon effects.
- 2D interlayer AF, bulk interlayer FM

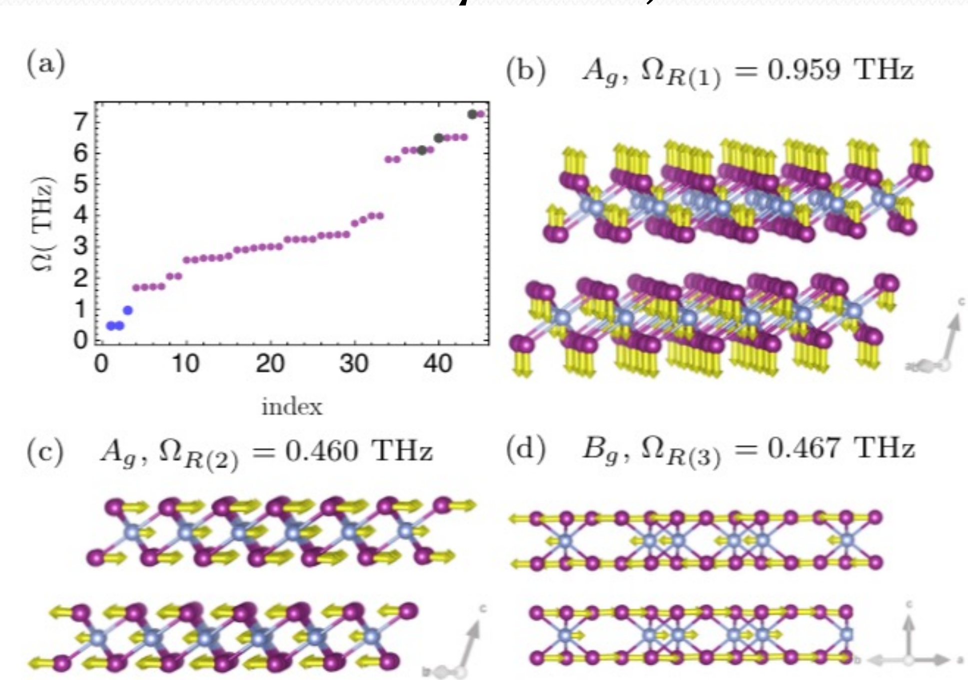

$$V[Q_{\mathrm{IR}}, Q_{\mathrm{R}(i)}] = \frac{1}{2}\Omega_{\mathrm{IR}}^2 Q_{\mathrm{IR}}^2 + \sum_{i=1}^{3} \frac{1}{2}\Omega_{\mathrm{R}(i)}^2 Q_{\mathrm{R}(i)}^2 + \sum_{i=1}^{2} \frac{\beta_i}{3} Q_{\mathrm{R(i)}}^3 + Q_{\mathrm{IR}}^2 \sum_{i=1}^{2} \gamma_i Q_{\mathrm{R(i)}} + \delta Q_{\mathrm{R}(1)}^2 Q_{\mathrm{R}(2)} + \epsilon Q_{\mathrm{R}(1)} Q_{\mathrm{R}(2)}^2 + Q_{\mathrm{R}(3)}^2 \sum_{i=1}^{2} \zeta_i Q_{\mathrm{R(i)}}.$$

$$Q_{\mathrm{R}}(t) = \frac{\gamma\pi (Z^* E_0 \tau^3)^2}{(4\Omega_{\mathrm{IR}}^2 - \Omega_{\mathrm{R}}^2)} \frac{\Omega_{\mathrm{IR}}^2}{\Omega_{\mathrm{R}}^2} \left(\Omega_{\mathrm{R}}^2 \cos(2\Omega_{\mathrm{IR}} t) + 2(\Omega_{\mathrm{IR}}^2 - \Omega_{\mathrm{R}}^2)\cos(\Omega_{\mathrm{R}} t) + \Omega_{\mathrm{R}}^2 - 4\Omega_{\mathrm{IR}}^2 \right).$$

M. Rodriguez-Vega, Z. Lin, A. Leonardo, A. Ernst, G. Chaudhary, M. G. Vergniory, and GAF, PRB Rapid (2020).

Phonon mediated dimensional crossover in CrI_3

- Idea: modulate interlayer exchange coupling via nonlinear phonon effects.
- 2D interlayer AF, bulk FM

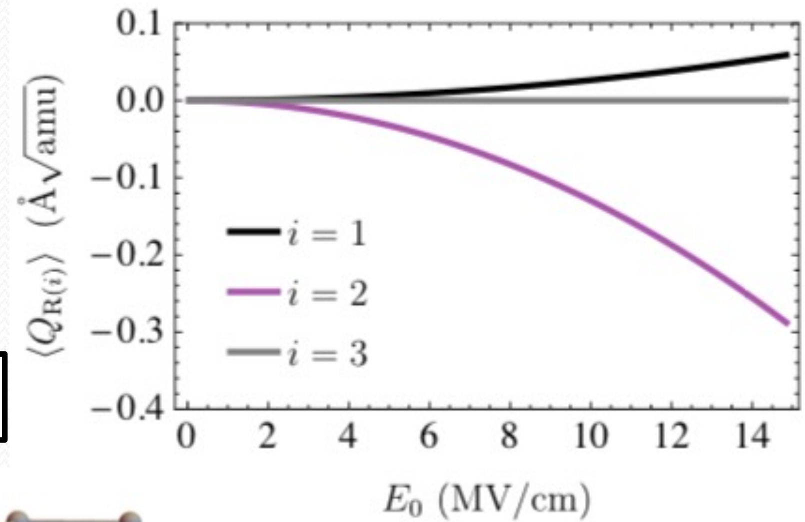

$$\mathcal{H}_{\text{intra}} = \sum_{\langle ij \rangle \in \lambda\mu(\nu)} \mathcal{J} \mathbf{s}_i \cdot \mathbf{s}_j + K s_i^\nu s_j^\nu + \Gamma \left(s_i^\lambda s_j^\mu + s_i^\mu s_j^\lambda \right)$$

$$\mathcal{H}_{\text{inter}} = \frac{1}{2} \sum_{ij \in \text{int.}} J_{ij} \mathbf{s}_i \cdot \mathbf{s}_j$$

$$\boxed{J^{\text{eff}} = J^0 + \delta J \hat{\boldsymbol{\delta}} \cdot \langle \boldsymbol{u}_{\text{R}} \rangle}$$

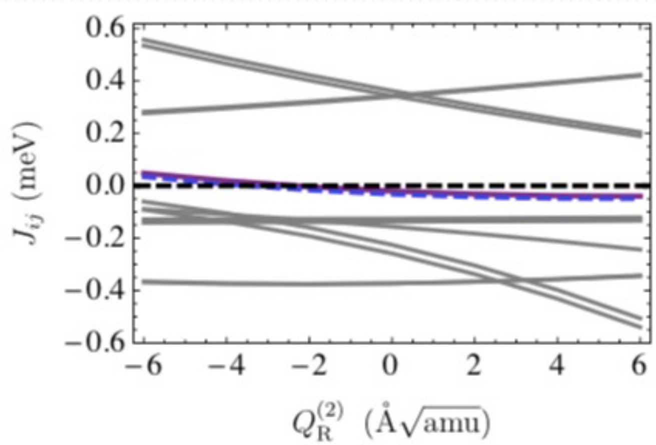

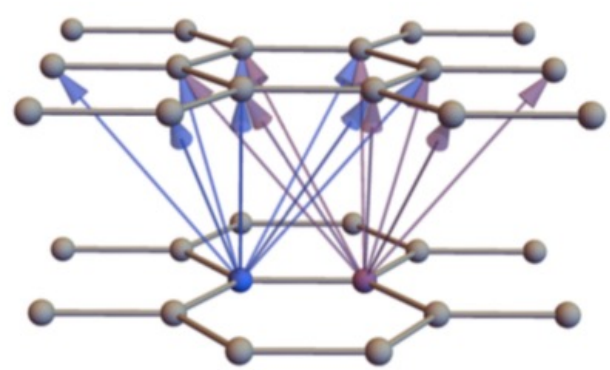

Change sign of interlayer Coupling: AFM → FM

M. Rodriguez-Vega, Z. Lin, A. Leonardo, A. Ernst, G. Chaudhary, M. G. Vergniory, and GAF, PRB Rapid (2020).

Phonon mediated magnetic transition and topological band transition in MnX_2Te_4 , X=Bi, Sb bilayers

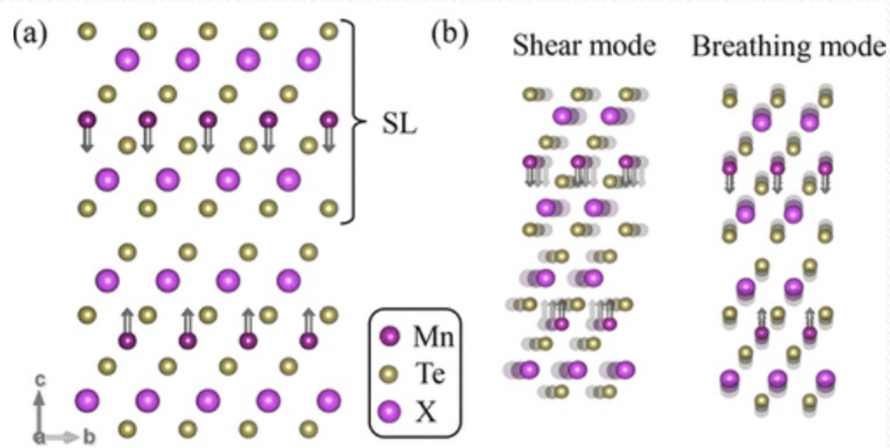

T_C~20K

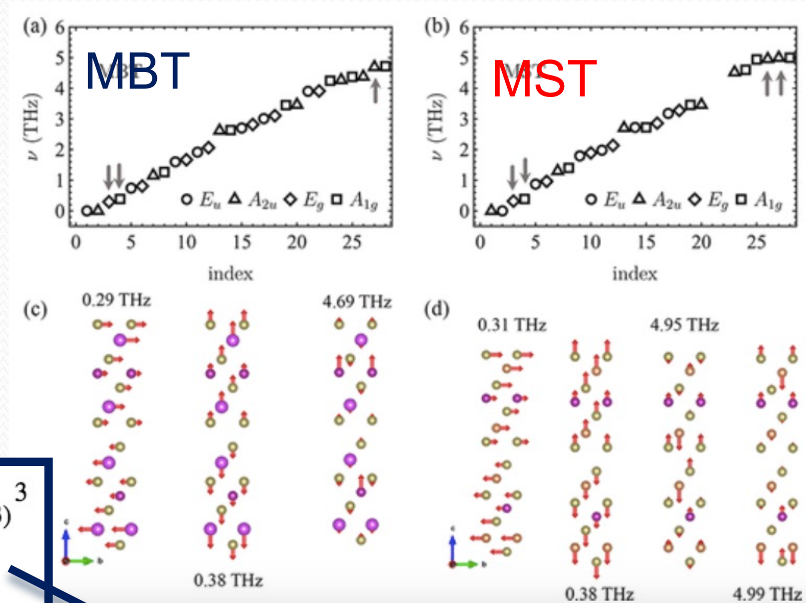

$$V[Q_{\mathrm{IR}}, Q_{\mathrm{R}(3)}, t] = \frac{1}{2}\Omega_{\mathrm{IR}}{}^2 Q_{\mathrm{IR}}{}^2 + \frac{1}{2}\Omega_{\mathrm{R}(3)}{}^2 Q_{\mathrm{R}(3)}{}^2 + \gamma_3 Q_{\mathrm{IR}}{}^2 Q_{\mathrm{R}(3)} + \frac{1}{3}\beta_3 Q_{\mathrm{R}(3)}{}^3 + \boldsymbol{Z}^{*}\cdot \boldsymbol{E}_0 \sin(\Omega t) F(t) Q_{\mathrm{IR}}$$

MBT

$$V[\{Q_{\mathrm{IR}(i)}\}, Q_{\mathrm{R}(3)}, t] = \sum_{i=1}^{2} \frac{1}{2}\Omega_{\mathrm{IR}(i)}{}^2 Q_{\mathrm{IR}(i)}{}^2 + \frac{1}{2}\Omega_{\mathrm{R}(3)}{}^2 Q_{\mathrm{R}(3)}{}^2 + \gamma_{1,3} Q_{\mathrm{IR}(1)}{}^2 Q_{\mathrm{R}(3)} + \gamma_{2,3} Q_{\mathrm{IR}(2)}{}^2 Q_{\mathrm{R}(3)} + \gamma_{1,2,3} Q_{\mathrm{IR}(1)} Q_{\mathrm{IR}(2)} Q_{\mathrm{R}(3)} + \frac{1}{3}\beta_3 Q_{\mathrm{R}(3)}{}^3 + [\boldsymbol{Z}_1^{*} Q_{\mathrm{IR}(1)} + \boldsymbol{Z}_2^{*} Q_{\mathrm{IR}(2)}]\cdot \boldsymbol{E}_0 \sin(\Omega t) F(t)$$

MST

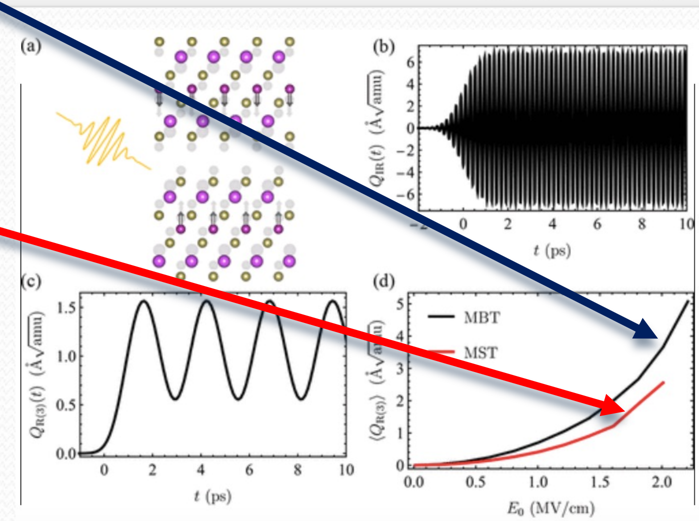

M. Rodriguez-Vega, Z. Lin, A. Leonardo, A. Ernst,
M. G. Vergniory, and GAF, JPCL (2022).

Phonon mediated magnetic transition and topological band transition in MnX_2Te_4 , X=Bi, Sb bilayers

$$\mathcal{H} = \mathcal{H}_{\text{intra}} + \mathcal{H}_{\text{inter}} \qquad \mathcal{H}_{\text{intra}} = -\sum_{ij} J_{ij}\mathbf{S}_i \cdot \mathbf{S}_j - D\sum_i (S_i^z)^2 \qquad \mathcal{H}_{\text{inter}} = -J_c \sum_{\langle ij \rangle} \mathbf{S}_i \cdot \mathbf{S}_j$$

$$J^{\text{eff}} = J^0 + \delta J \hat{\boldsymbol{\delta}} \cdot \langle \boldsymbol{u}_{\text{R}} \rangle$$

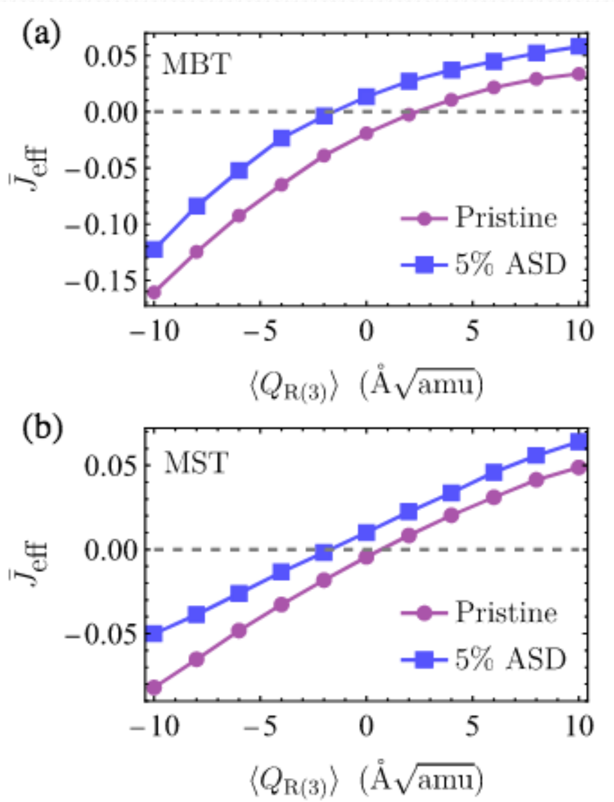

T_C~20K

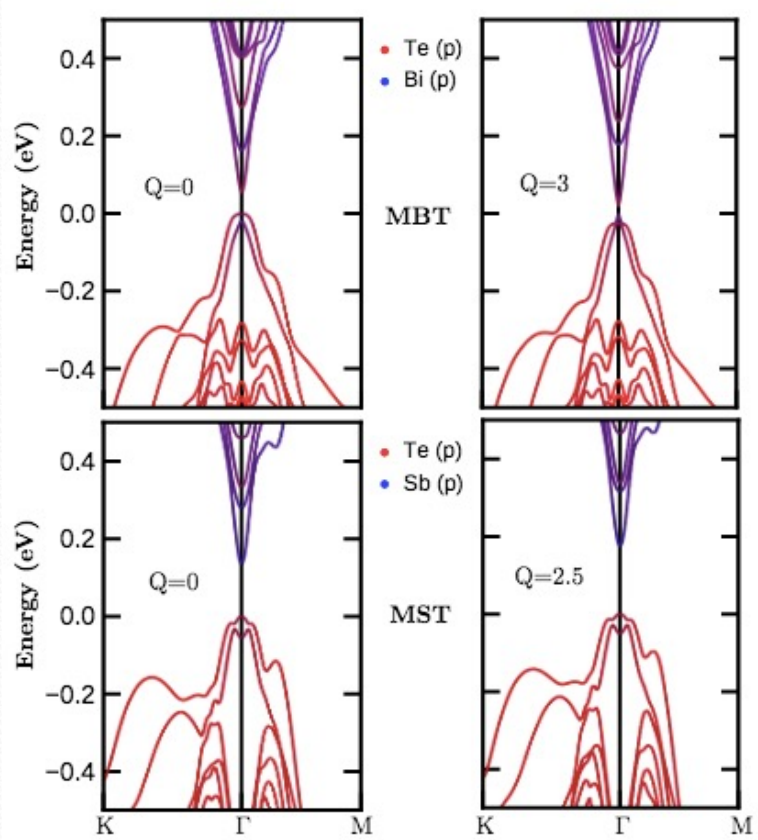

M. Rodriguez-Vega, Z. Lin, A Leonardo, A. Ernst, M. G. Vergniory, and GAF, JPCL (2022).

Advertisement: Swati Chaudhary

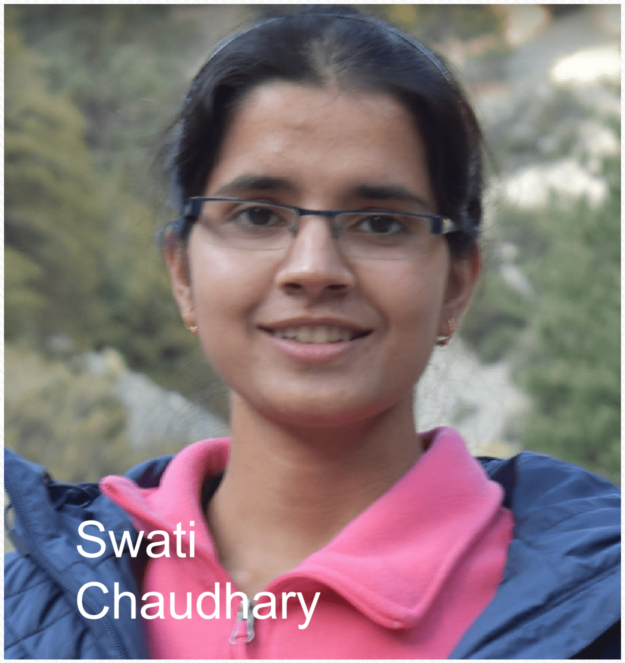

Chiral phonons with a giant phonon Zeeman effect

Thursday, 16:50 Talk

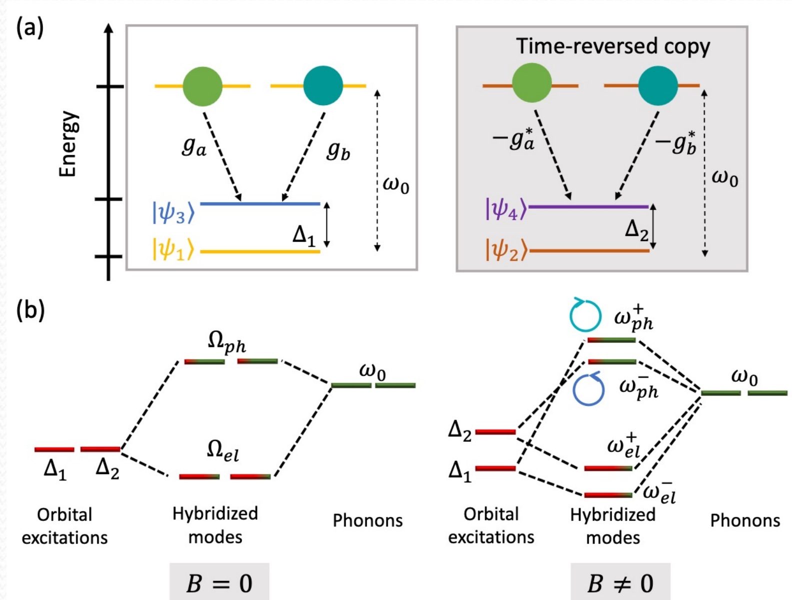

Nonlinear optical responses in Weyl systems: a probe of quantum geometry

$$T_{\alpha\beta}^{nn'} = g_{\alpha\beta}^{nn'} + i\Omega_{\alpha\beta}^{nn'}$$

Quantum geometry

$$g_{\alpha\beta}^{nn'} = Re \sum_{m \neq n,n'} [\langle u_n | i\partial_{k_\alpha} | u_m \rangle \langle u_m | i\partial_{k_\beta} | u_{n'} \rangle]$$ quantum metric

$$\Omega_{\alpha\beta}^{nn'} = -2Im \sum_{m \neq n,n'} [\langle u_n | i\partial_{k_\alpha} | u_m \rangle \langle u_m | i\partial_{k_\beta} | u_{n'} \rangle]$$ Berry curvature

- Focus on the bulk photogalvanic effects where a dc photocurrent is generated in systems with broken inversion symmetry.
- The photocurrent reveals the quantum geometric structure of the band structure and has two physical origins during optical excitation: (i) A transition in the electron position, leading to a "shift current" and (ii) a transition of the electron velocity leading to an "injection current".

J. Ahn, G.-Y. Guo, and N. Nagaosa, *PRX* **10**, 0411042 (2020).
J. Ahn, G.-Y. Guo, N. Nagaosa and A. Vishwanath *Nat. Phys.* **18**, 290 (2022).

Weyl Systems: Fundamentals

- Topologically protected metal with nodal points exhibiting linear band dispersion with connected surface Fermi arcs.

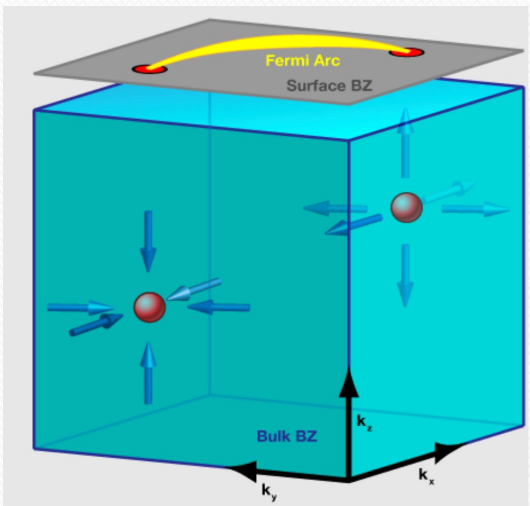

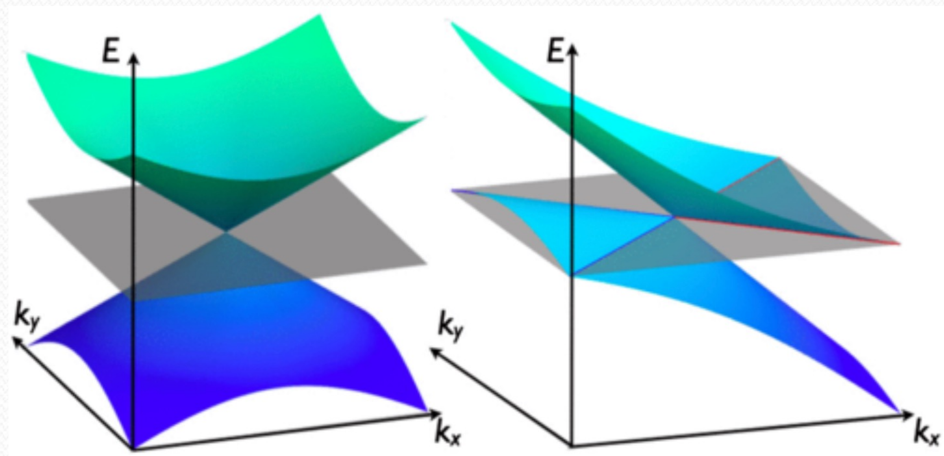

Type I Type II

- Weyl materials require broken time-reversal and/or broken inversion symmetry.

L. Balents, *Physics* **4**, 36 (2011); X. Wan, A. M. Turner, A. Vishwanath, and S. Y. Savrasov *Phys. Rev. B* **83**, 205101 (2011); N. P. Armitage, E. J. Mele, and Ashvin Vishwanath Rev. Mod. Phys. **90**, 015001 (2018); B. Yan and C. Felser, *Ann. Rev. Cond. Mat*. **8**, 337 (2017).

Predicted quantized photogalvanic response

- Electrical currents induced as a nonlinear response to illumination with light.

$$\frac{1}{2}\left[\frac{dj_{\circlearrowleft}}{dt} - \frac{dj_{\circlearrowright}}{dt}\right] = \frac{2\pi e^3}{h^2 c\epsilon_0} I C_i = \frac{4\pi\alpha e}{h} I C_i$$

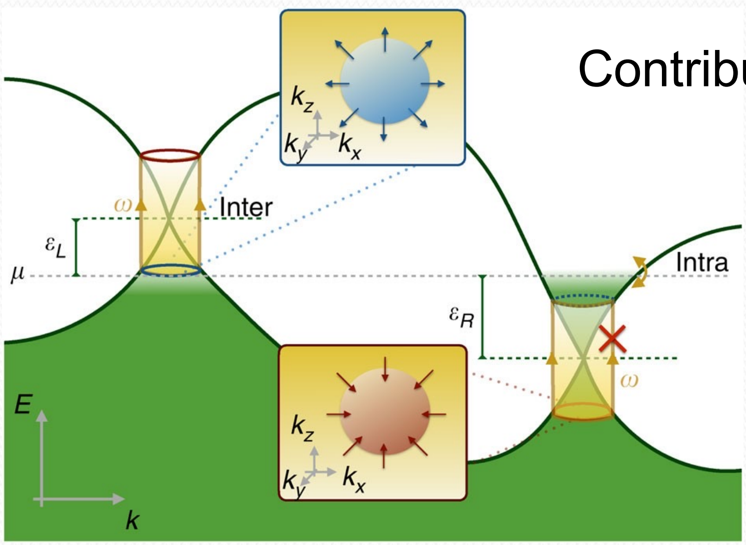

Contributions from a single node

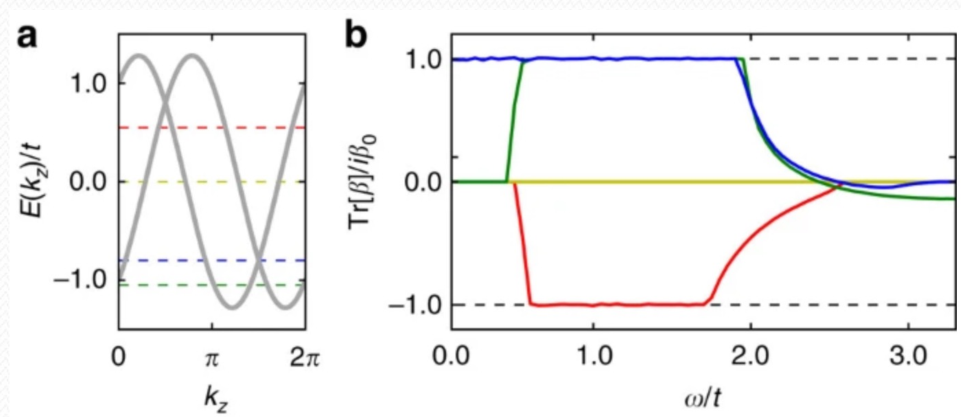

F. de Juan, A. G. Grushin, T. Morimoto, J. E. Moore, *Nat. Comm.* **8**, 15995 (2017).
C.-K. Chan, N. H. Lindner, G. Refael, and P. A. Lee *Phys. Rev. B* **95**, 041104(R) (2017).

Circular photogalvanic effect (CPGE) in RhSi

- No sharp quantization as predicted in theory, but suggestive.

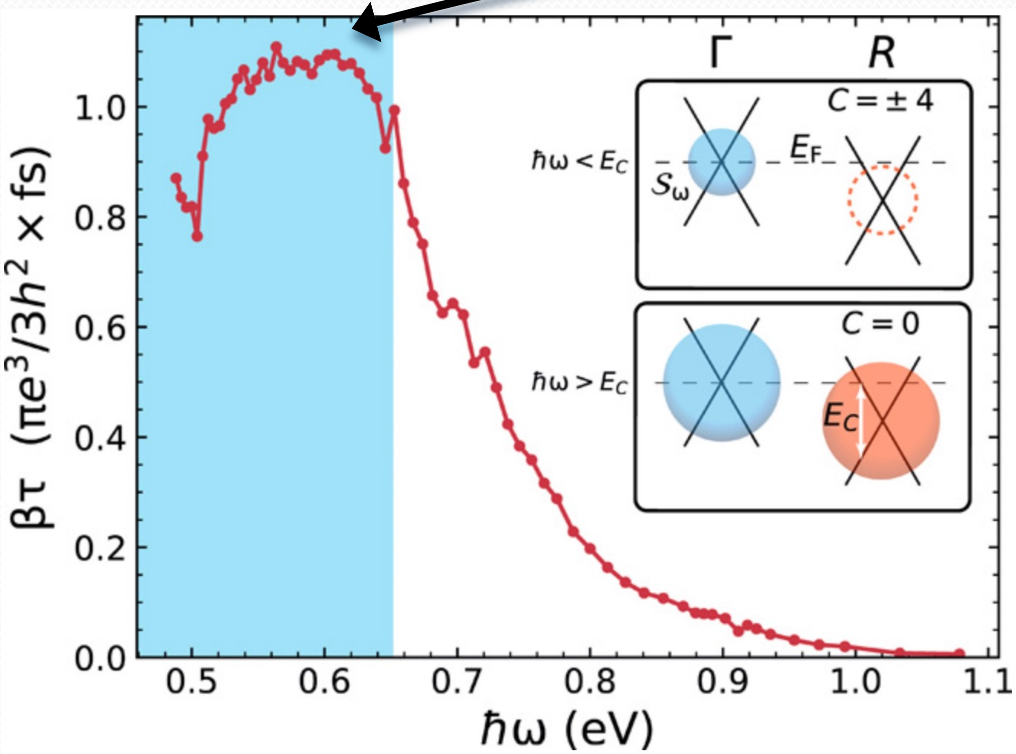

Nearly quantized, but rather poor compared to quantum Hall effects.

D. Rees, K. Manna, B. Lu, T. Morimoto, H. Borrmann, C. Felser, J. E. Moore, D. H. Torchinsky, and J. Orenstein, *Sci. Adv*. **6**, (2020).
See also: Z. Ni, B. Zu, …L. Wu, *npj Quantum Materials* **5**, 96 (2020).

Nonlinear response: Role of quantum geometry

$$j^a_{dc} = \sigma^{abc}(\omega) E_b(\omega) E_c(-\omega),$$

$$\sigma^{abc}(0;\omega,-\omega) = \sigma^{abc}_{\text{shift}} + \sigma^{abc}_{\text{inj}}$$

$$\sigma^{abc}_{\text{shift}} = \frac{-i\pi e^3}{\hbar^2} \int_{\mathbf{k}} \sum_{n>m} f_{nm} \left(r^b_{nm} r^c_{mn;a} - r^c_{mn} r^b_{nm;a} \right) \times \delta(\omega_{nm} - \omega),$$

$$\sigma^{abc}_{\text{inj}} = \tau \frac{2\pi e^3}{\hbar^2} \int_{\mathbf{k}} \sum_{n>m} f_{nm} \Delta^a_{nm} r^b_{nm} r^c_{mn} \delta(\omega_{nm} - \omega),$$

Quantum geometry expressed in "r":

$$r^b_{nm;a} = \frac{\partial r^b_{nm}}{\partial k_a} - i(\xi^a_{nn} - \xi^a_{mm}) r^b_{nm}$$

$$\xi^a_{nn} = \langle n | i \frac{\partial}{\partial k_a} | n \rangle$$

$$r^b_{nm} = \langle n | i \frac{\partial}{\partial k_b} | m \rangle$$

J. Ahn, G.-Y. Guo, and N. Nagaosa, *PRX* **10**, 0411042 (2020).

J. Ahn, G.-Y. Guo, N. Nagaosa and A. Vishwanath *Nat. Phys.* **18**, 290 (2022).

A. Raj, S. Chaudhary, GAF *Phys. Rev. Res.* 6, 013048 (2024)

Model Hamiltonian and Quantization of CPGE: Analytical Results

Consider nodes with n=1,2,3 (and 4 with different form)

$$\mathcal{H}_n = \begin{pmatrix} u_z k_z + u_t k_z - \mu & \varepsilon_0(\zeta_x \tilde{k}_x - i\zeta_y \tilde{k}_y)^n \\ \varepsilon_0(\zeta_x \tilde{k}_x + i\zeta_y \tilde{k}_y)^n & -u_z k_z + u_t k_z - \mu \end{pmatrix}$$

Chirality:

$$\chi = \mathrm{sgn}(u_z \zeta_x \zeta_y)$$

JDOS	$\frac{k_0^2}{8\pi^2 \lvert u_z \rvert} \frac{1}{n} (\frac{\omega}{2\varepsilon_0})^{2/n} \int_{\theta_1}^{\theta_2} \cos^{2/n-1}\theta \mathrm{d}\theta$	
Shift conductivity		Broken symmetries
$\sigma^{xzx} = -\sigma^{xxz} = \sigma^{yzy} = -\sigma^{yyz}$	$n \frac{i\,\mathrm{sgn}(u_z) e^3 k_0^2}{32\pi\hbar^2} (\sin^2\theta_2 - \sin^2\theta_1) \frac{1}{\omega}$	M_z, TRS
$\sigma^{xyz} = \sigma^{xzy} = -\sigma^{yzx} = -\sigma^{yxz}$	$n \frac{\mathrm{sgn}(u_z \zeta_x \zeta_y) e^3 k_0^2}{32\pi\hbar^2} (\sin\theta_2 \cos^2\theta_2 - \sin\theta_1 \cos^2\theta_1) \frac{1}{\omega}$	M_x, M_y, M_z
Injection conductivity		
$\sigma^{zxy} = -\sigma^{zyx}$	$n \frac{i\tau\,\mathrm{sgn}(u_z \zeta_x \zeta_y) e^3 k_0^2}{24\pi\hbar^2} (\sin^3\theta_1 - \sin^3\theta_2)$	M_x, M_y, M_z
$\sigma^{yzy} = \sigma^{yyz} = \sigma^{xzx} = \sigma^{xxz}$	$n \frac{\tau\,\mathrm{sgn}(u_z) e^3 k_0^2}{64\pi\hbar^2} (\cos^4\theta_1 - \cos^4\theta_2)$	M_z, TRS
$\sigma^{xyz} = -\sigma^{xzy} = \sigma^{yzx} = -\sigma^{yxz}$	$n \frac{i\tau\,\mathrm{sgn}(u_z \zeta_x \zeta_y) e^3 k_0^2}{48\pi\hbar^2} (3\sin\theta_1 - \sin^3\theta_1 - 3\sin\theta_2 + \sin^3\theta_2)$	M_x, M_y, M_z
$\sigma^{zxx} = \sigma^{zyy}$	$n \frac{\tau\,\mathrm{sgn}(u_z) e^3 k_0^2}{256\pi\hbar^2} [-6\cos(2\theta_1) + \cos^2(2\theta_1) + 6\cos(2\theta_2) - \cos^2(2\theta_2)]$	M_z, TRS
σ^{zzz}	$\frac{\tau u_z^2\,\mathrm{sgn}(u_z) e^3 k_0^2}{2^{2+2/n} \varepsilon_0^{2/n} (1+n)\pi\hbar^2 \omega^{2-2/n}} (\cos^{2+2/n}\theta_2 - \cos^{2+2/n}\theta_1)$	M_z, TRS

$$\frac{2\pi}{i\tau e^3 k_0^2/\hbar^2} \epsilon_{abc} \sigma^{abc}_{\mathrm{inj}} = -n\,\mathrm{sgn}(u_z \zeta)$$

A. Raj, S. Chaudhary, GAF *PRR* 6, 013048 (2024)

Quality of quantization in n=2 low-energy model versus tight-binding model

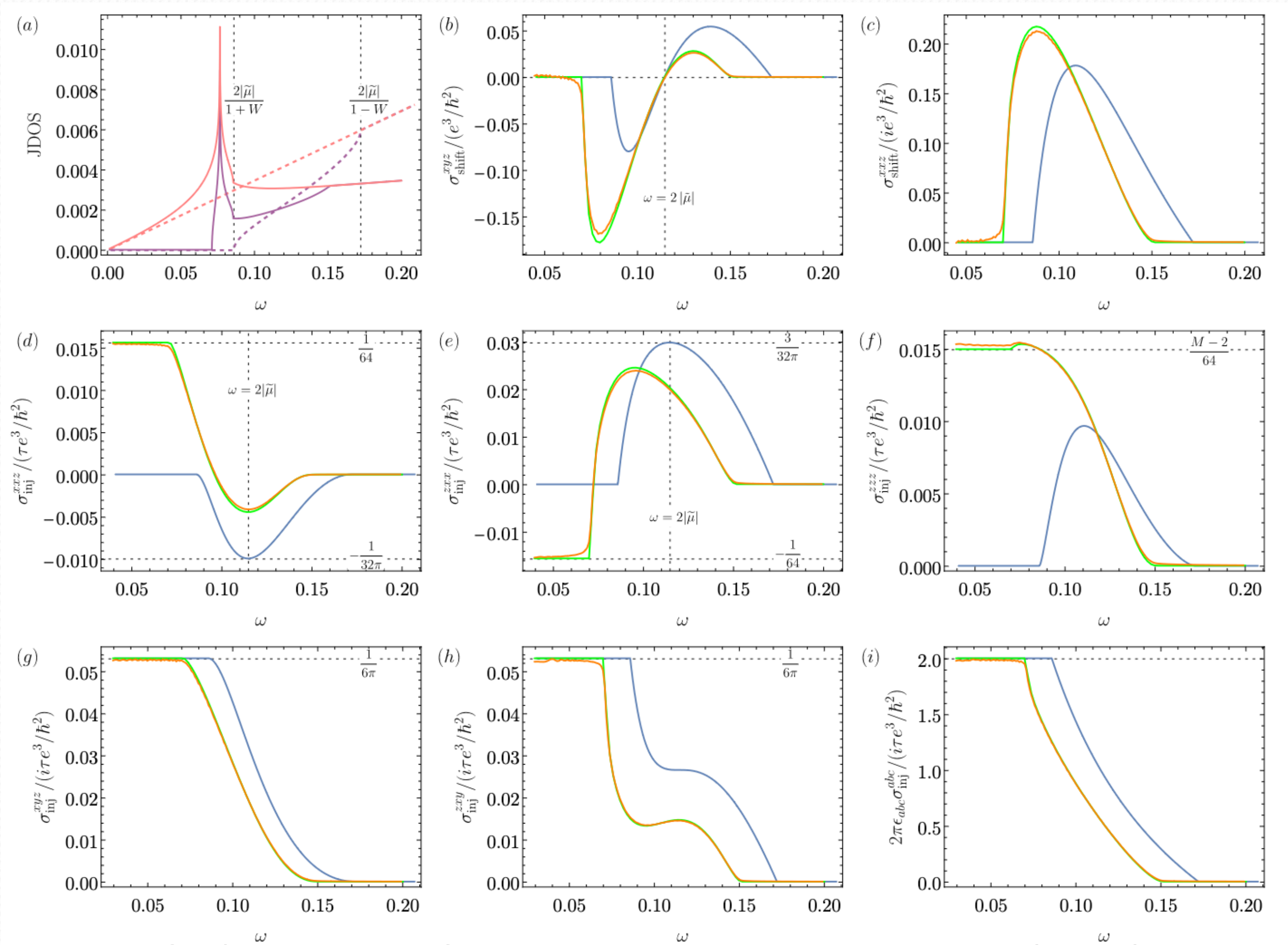

Tight-binding

Low-energy

Low-energy with corrections

The low-energy corrections produce remarkably accurate results.

A. Raj, S. Chaudhary, GAF *Phys. Rev. Res.* 6, 013048 (2024)

Quality of quantization in n=2 full 4-band model compared to low-energy theory

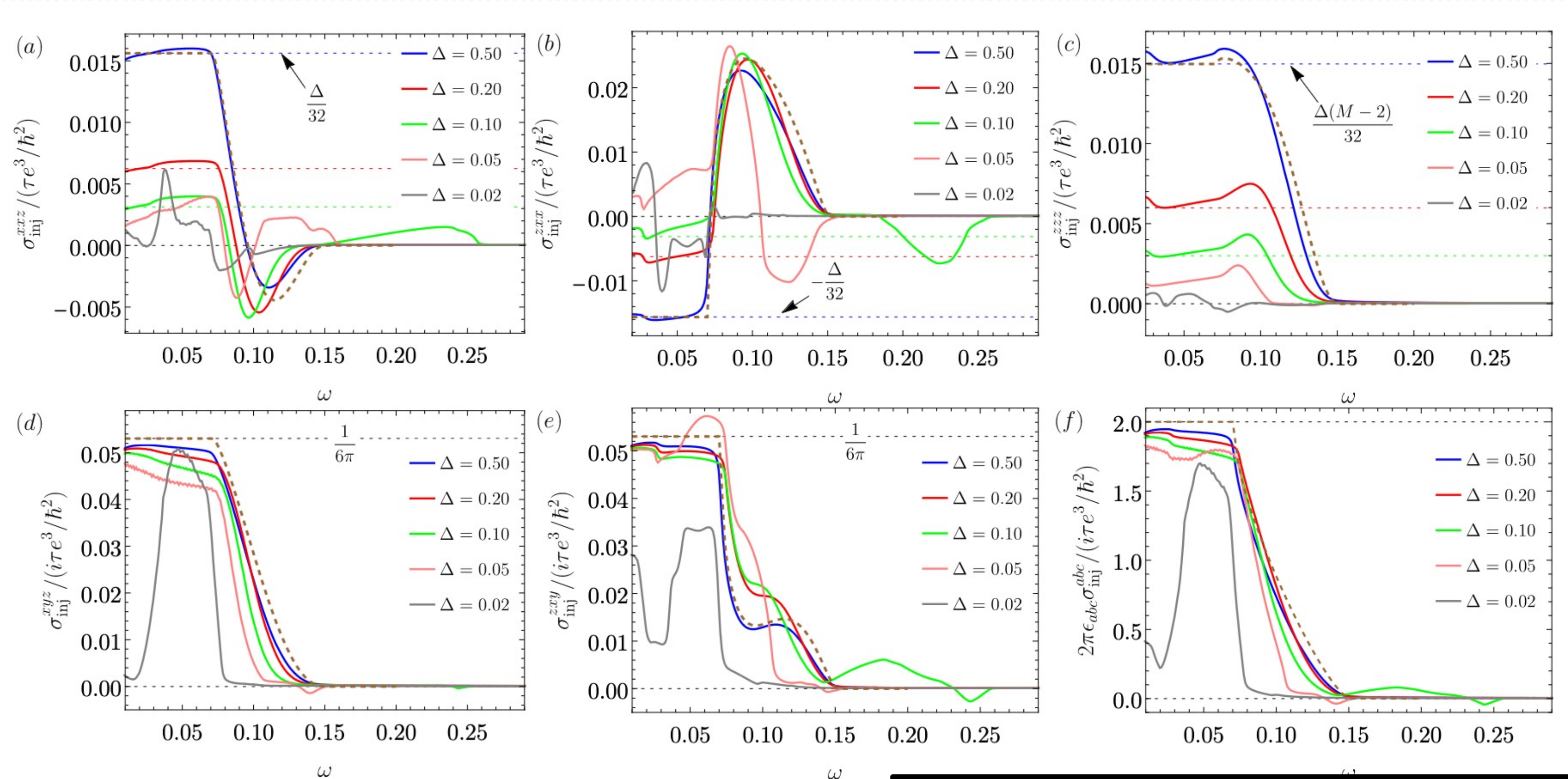

- - - Dotted curve is for 2-band model.

A. Raj, S. Chaudhary, GAF *PRR* 6, 013048 (2024)

$$\begin{aligned}\mathcal{H}^{4b} = t\big(&\sin(k_x)\tau_x + \sin(k_y)\tau_y \\ &+ (M - \cos(k_x) - \cos(k_y) - \cos(k_z))\tau_z \\ &+ \Delta\,(\tau_x\sigma_x + \tau_y\sigma_y) + g\sin(k_z)\tau_z\sigma_z\big) - \mu,\end{aligned}$$

Broken TRS

Gap between highest occupied and lowest unoccupied

New Weyl results for n=4

Two-band lattice model with n=4 Weyl points:

$$\mathcal{H}_4 = -2c_1(\cos(k_x)+\cos(k_y)+\cos(k_z))\sigma_0 + 2c_2\Big(\sqrt{3}(\cos(k_y)-\cos(k_x))\sigma_x - (\cos(k_x)+\cos(k_y)-2\cos(k_z))\sigma_z\Big) + c_3\sin(k_x)\sin(k_y)\sin(k_z)\sigma_y - \widetilde{\mu}\sigma_0,$$

Effective low-energy Hamiltonian near the Γ point:

$$\mathcal{H}_4^{\Gamma} = c_1\left(k_x^2+k_y^2+k_z^2\right)\sigma_0 + c_2\Big(\sqrt{3}\left(k_x^2-k_y^2\right)\sigma_x + \left(k_x^2+k_y^2-2k_z^2\right)\sigma_z\Big) + c_3 k_x k_y k_z \sigma_y - \mu\sigma_0,$$

Dotted curves are low-energy model

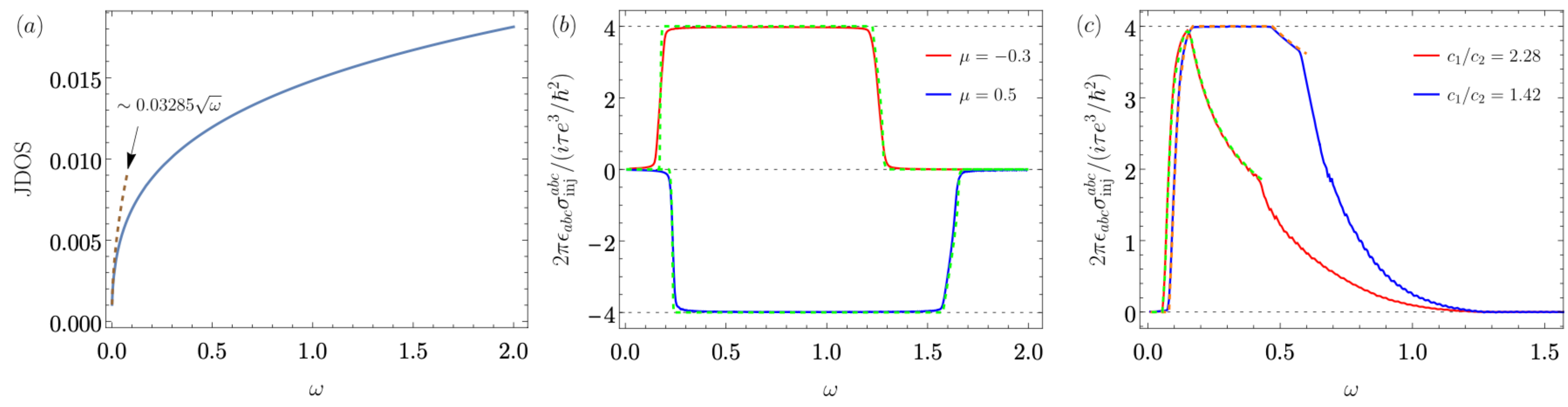

Strong quantization of CPGE within the two-band model.

A. Raj, S. Chaudhary, GAF *Phys. Rev. Res.* 6, 013048 (2024)

Summary of non-linear optical responses in Weyl systems

- Quantization of injection current reveals quantum geometry of multi-Weyl systems, but does not survive beyond 2-bands.
- Investigated the dependence of the shift & injection currents on the topological charge, tilt and chemical potential within full multi-band and low-energy approx.
- Information about the chiral charge of Weyl points and type-I/type-II character can be inferred from a measurement of different components of the second order conductivity tensor.
- We provided new analytical results and analysis for the case of chiral charge 4 (the largest stable value permitted on a lattice).

Candidate Topological Superconductor: $4Hb\text{-}TaS_2$

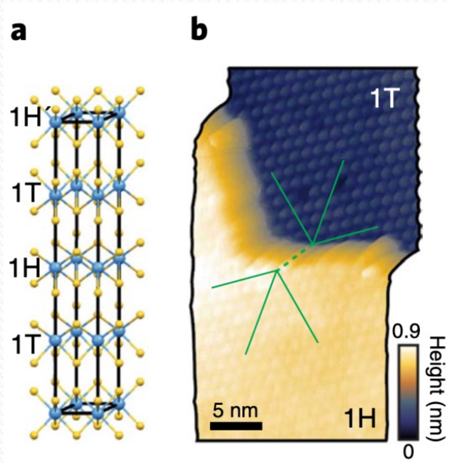

nature physics
ARTICLES
https://doi.org/10.1038/s41567-021-01376-z
Check for updates

Evidence of topological boundary modes with topological nodal-point superconductivity

Abhay Kumar Nayak[1,5], Aviram Steinbok[1,5], Yotam Roet[1,5], Jahyun Koo[1], Gilad Margalit[1], Irena Feldman[2], Avior Almoalem[2], Amit Kanigel[2], Gregory A. Fiete[3,4], Binghai Yan[1], Yuval Oreg[1], Nurit Avraham[1]✉ and Haim Beidenkopf[1]✉

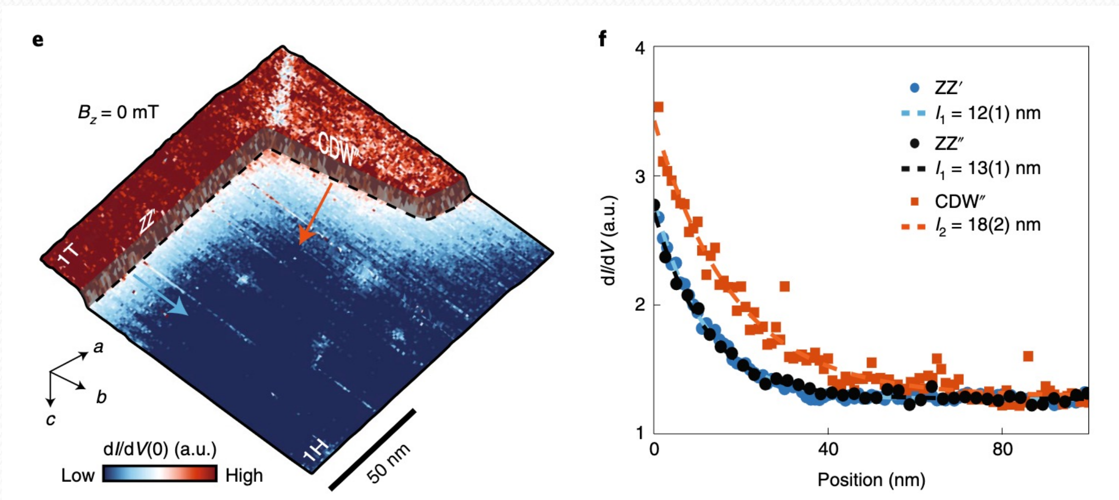

Topological edge mode?

Metallic-like boundary states seen in zero-bias conductance.

Optical Probe of Candidate Topological Superconductor: 4Hb-TaS_2

$$H_{SC}(\mathbf{k}) = \begin{bmatrix} H_0(\mathbf{k}) & \Delta \\ \Delta^\dagger & -H_0(-\mathbf{k})^T \end{bmatrix}$$

$$\psi_{\mathbf{k}}^T = (d_{z^2,\uparrow}, d_{xy,\uparrow}, d_{x^2-y^2,\uparrow}, d_{z^2,\downarrow}, d_{xy,\downarrow}, d_{x^2-y^2,\downarrow})$$

$$\Delta = \begin{bmatrix} 0 & \Delta_4 & i\Delta_4 & \Delta_1 & 0 & 0 \\ -\Delta_4 & 0 & 0 & 0 & \Delta_2 & i\Delta_3 \\ -i\Delta_4 & 0 & 0 & 0 & -i\Delta_3 & \Delta_2 \\ -\Delta_1 & 0 & 0 & 0 & \Delta_4 & -i\Delta_4 \\ 0 & -\Delta_2 & i\Delta_3 & -\Delta_4 & 0 & 0 \\ 0 & -i\Delta_3 & -\Delta_2 & i\Delta_4 & 0 & 0 \end{bmatrix}$$

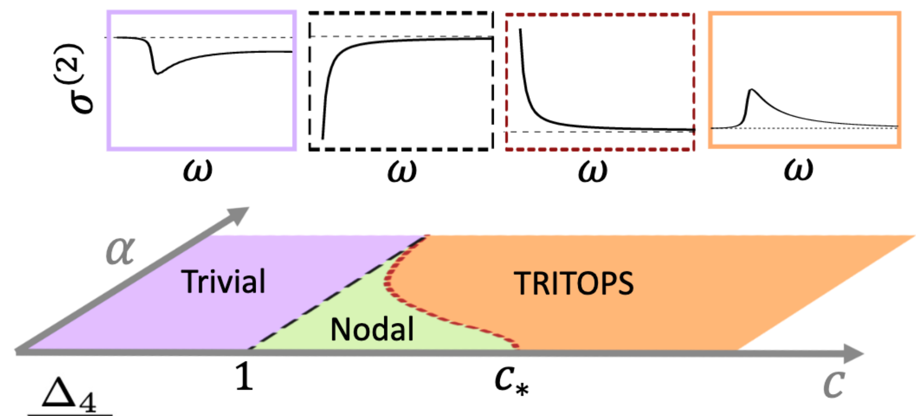

$$c = \frac{\Delta_4}{\zeta \Delta_1}$$

G. Margalit, E. Berg, and Y. Oreg, Ann. Phys. 345, 168561 (2021)

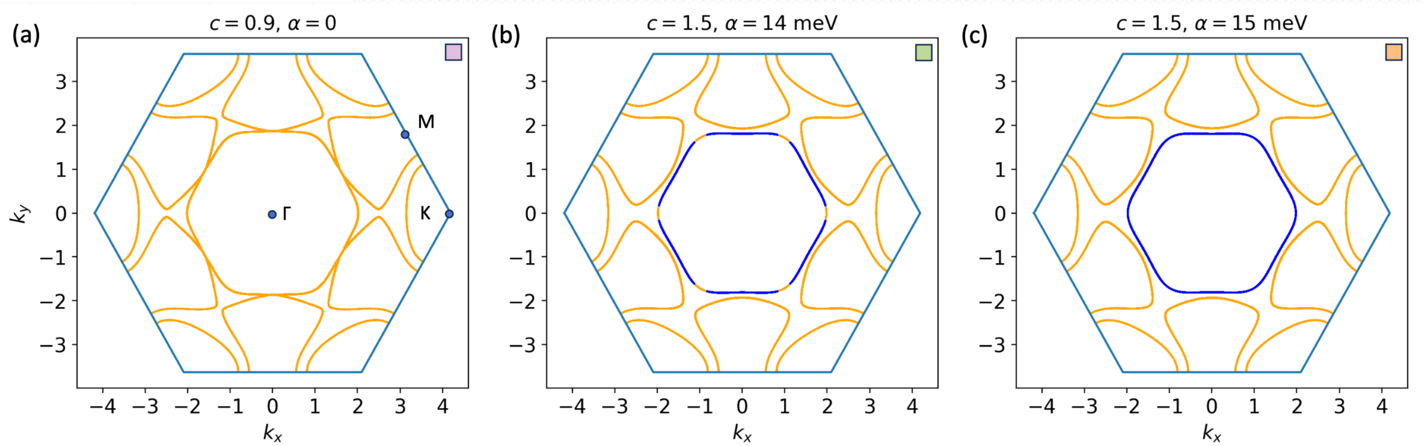

A. Raj, A. Postlewaite, S. Chaudhary, and G. A. Fiete, *Phys. Rev. B* **109**,184514 (2024).

Optical Probe of Candidate Topological Superconductor: 4Hb-TaS_2

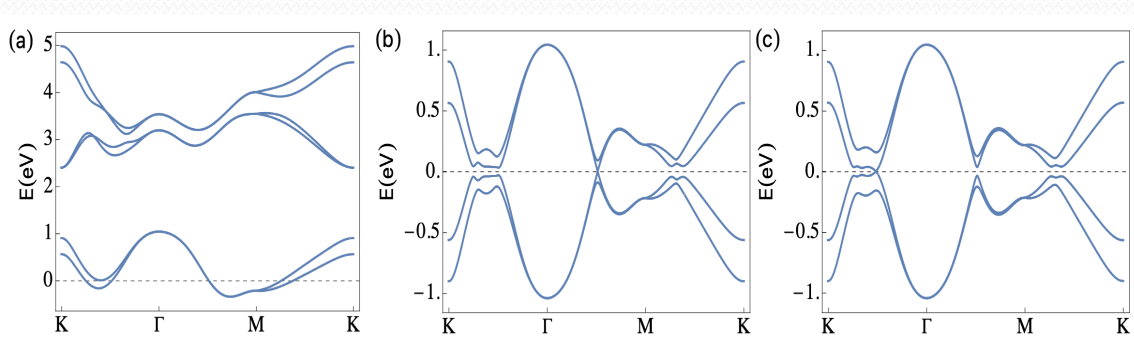

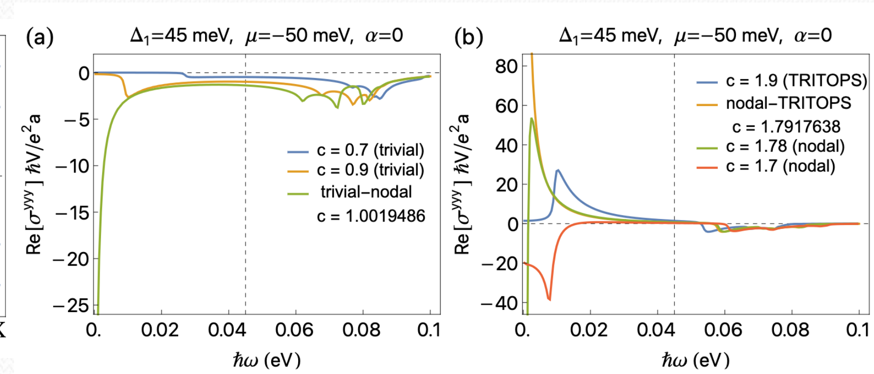

$$
\begin{aligned}
\sigma^{\alpha\beta\gamma}(\widetilde{\omega};\omega_1,\omega_2) = \int_{\mathrm{FBZ}} \frac{\mathrm{d}^2k}{(2\pi)^2}\, \frac{1}{2(i\omega_1-\eta)(i\omega_2-\eta)} \Bigg[& \sum_a \frac{1}{2} J^{\alpha\beta\gamma}_{aa} f_a + \sum_{a,b} \frac{1}{2}\left(\frac{J^{\alpha\beta}_{ab} J^{\gamma}_{ba} f_{ab}}{\omega_2+i\eta-E_{ba}} + \frac{J^{\alpha\gamma}_{ab} J^{\beta}_{ba} f_{ab}}{\omega_1+i\eta-E_{ba}} \right) \\
& + \sum_{a,b} \frac{1}{2} \frac{J^{\alpha}_{ab} J^{\beta\gamma}_{ba} f_{ab}}{\widetilde{\omega}+2i\eta-E_{ba}} + \sum_{a,b,c} \frac{1}{2} \frac{J^{\alpha}_{ab}}{\widetilde{\omega}+2i\eta-E_{ba}} \left(\frac{J^{\beta}_{bc} J^{\gamma}_{ca} f_{ac}}{\omega_2+i\eta-E_{ca}} - \frac{J^{\beta}_{ca} J^{\gamma}_{bc} f_{cb}}{\omega_2+i\eta-E_{bc}} \right) \\
& + \sum_{a,b,c} \frac{1}{2} \frac{J^{\alpha}_{ab}}{\widetilde{\omega}+2i\eta-E_{ba}} \left(\frac{J^{\gamma}_{bc} J^{\beta}_{ca} f_{ac}}{\omega_1+i\eta-E_{ca}} - \frac{J^{\gamma}_{ca} J^{\beta}_{bc} f_{cb}}{\omega_1+i\eta-E_{bc}} \right) \Bigg],
\end{aligned}
$$

$$c = \frac{\Delta_4}{\zeta \Delta_1}$$

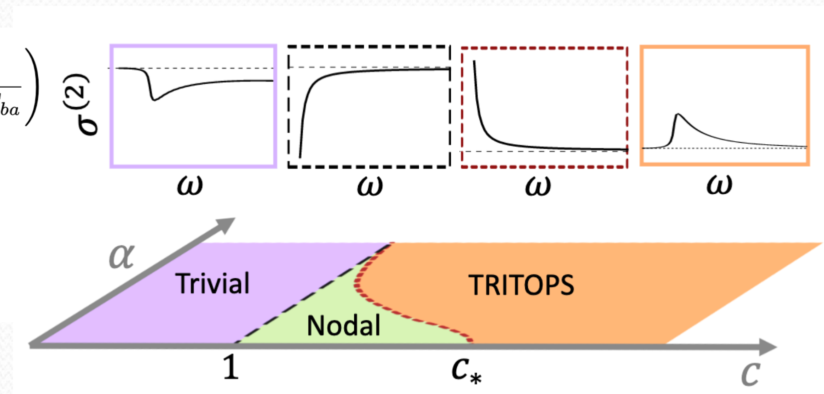

G. Margalit, E. Berg, and Y. Oreg, Ann. Phys. 345, 168561 (2021)

A. Raj, A. Postlewaite, S. Chaudhary, and G. A. Fiete, *Phys. Rev. B* **109**,184514 (2024).

Nonlinear optical responses in rhombohedral trilayer graphene

$$H^{\mathrm{ABC}}(\mathbf{k}) = -\begin{bmatrix} -\Delta-\Delta'/2 & \gamma_0 f(\mathbf{k}) & 0 & \gamma_3 f^*(\mathbf{k}) & 0 & \gamma_2 \\ \gamma_0 f^*(\mathbf{k}) & -\Delta+\Delta'/2 & \gamma_1 & 0 & 0 & 0 \\ 0 & \gamma_1 & \Delta'/2 & \gamma_0 f(\mathbf{k}) & 0 & \gamma_3 f^*(\mathbf{k}) \\ \gamma_3 f(\mathbf{k}) & 0 & \gamma_0 f^*(\mathbf{k}) & \Delta'/2 & \gamma_1 & 0 \\ 0 & 0 & 0 & \gamma_1 & \Delta+\Delta'/2 & \gamma_0 f(\mathbf{k}) \\ \gamma_2 & 0 & \gamma_3 f(\mathbf{k}) & 0 & \gamma_0 f^*(\mathbf{k}) & \Delta-\Delta'/2 \end{bmatrix},$$

$$f(\mathbf{k}) = e^{ik_y a/\sqrt{3}}\left[1 + 2e^{-3ik_y a/2\sqrt{3}}\cos\left(\frac{k_x a}{2}\right)\right],$$

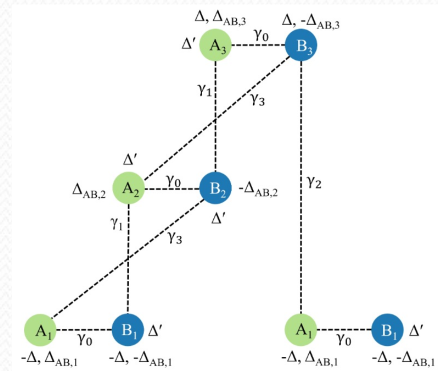

Δ=displacement field

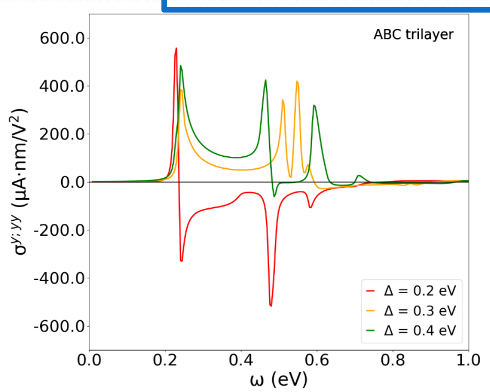

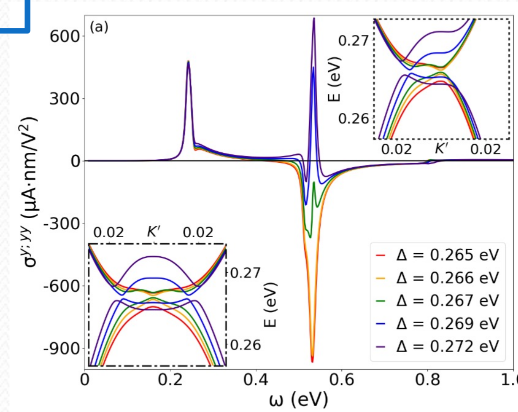

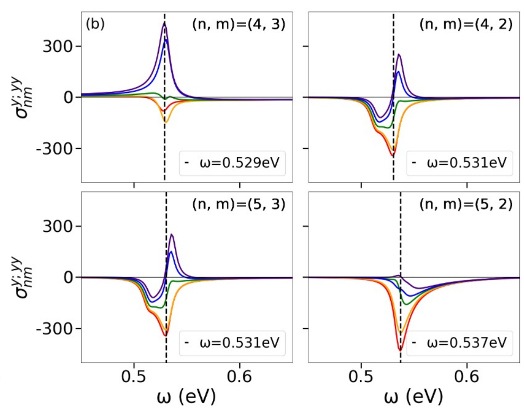

Focus in on band gap closing and band-resolved transitions

A. Postlewaite, A. Raj. S. Chuadhary, GAF arXiv:2407.03404

Nonlinear optical responses in rhombohedral trilayer graphene

$$\sigma_{nm}^{a;bc}(\omega) = \frac{2g_s\pi e^3}{\hbar^2}\int \frac{dk^2}{(2\pi)^2} f_{nm} I_{nm}^{a;bc}\delta(\omega_{nm}-\omega)$$

$$\mathcal{J}_{nm}(\omega) = \int \frac{dk^2}{(2\pi)^2}\delta(\omega_{nm}(\mathbf{k})-\omega)$$

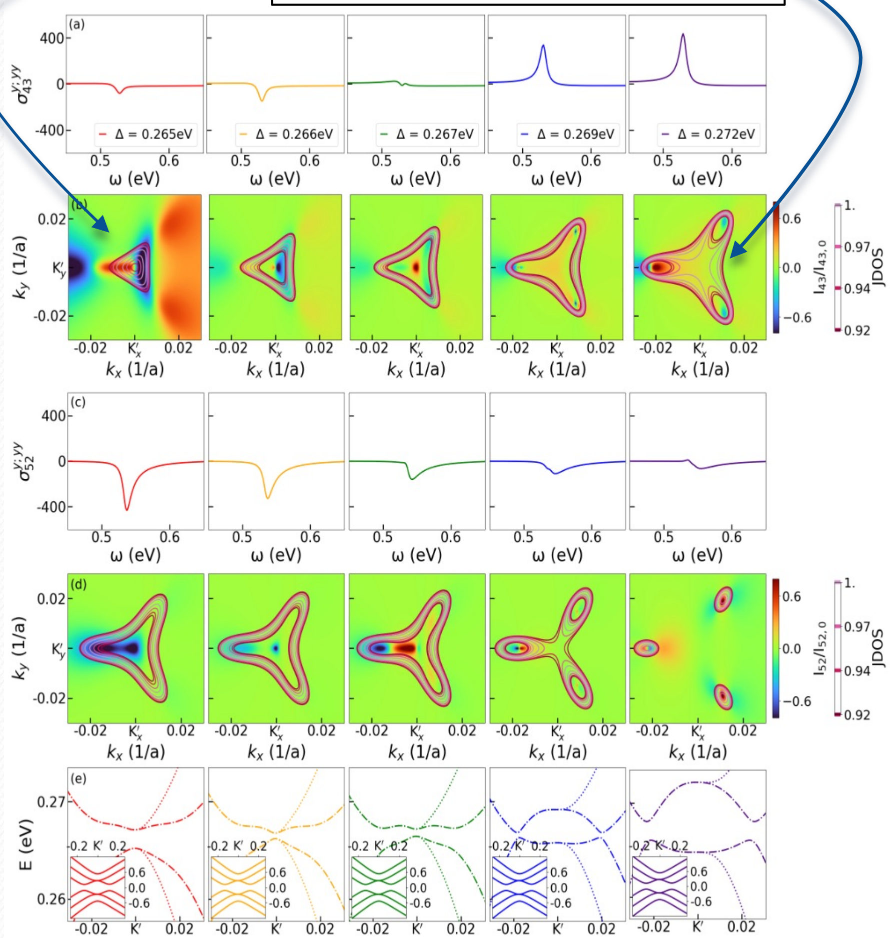

Quantum Metric

Berry Curvature

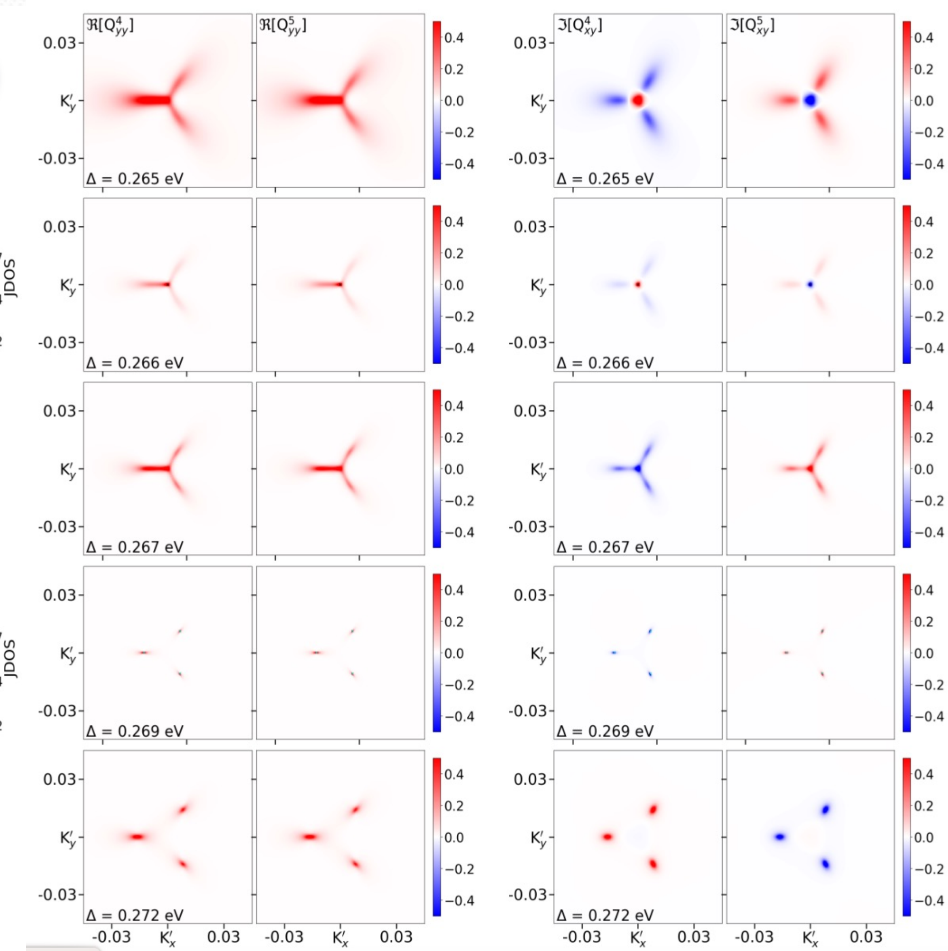

A. Postlewaite, A. Raj. S. Chaudhary, GAF arXiv:2407.03404

Δ=displacement field

Summary

- Tuning of effective twist angle with light.
- Nonlinear phononics can be used to change magnetic order, magnon band topology, and electronic band topology.
- Nonlinear optical responses of electronic systems can provide detailed information about band structure and nodal points of multi-Weyl systems.
- Nonlinear optical responses provide a tool to help diagnose topological superconductivity.
- Nonlinear optical responses provide important information about the quantum geometric tensor, but most often not a direct measure of it.

Wonderful Collaborators—Thank you!

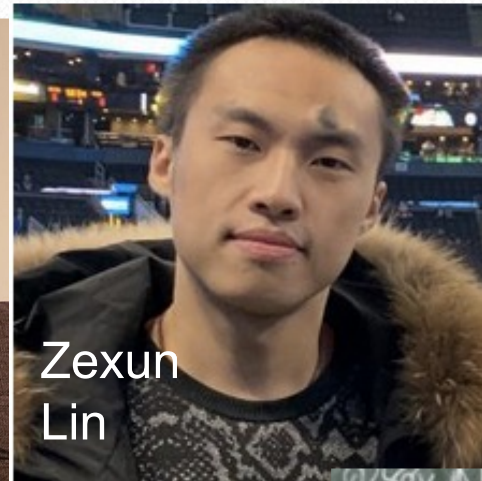

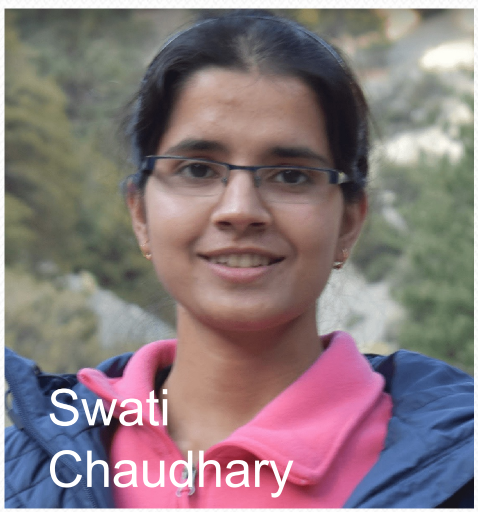

Weyl response to light: photocurrents

- Because of the chiral nature of Weyl fermions, there is a helicity-dependent interband absorption.

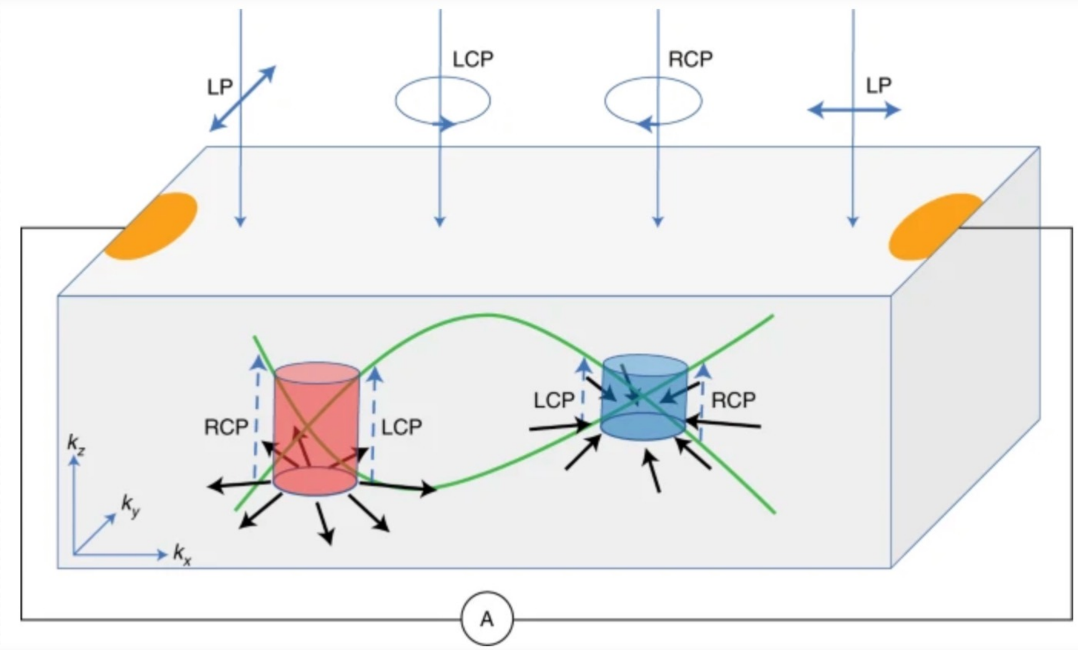

Band topology and quantum geometric properties of the bands are revealed in the nonlinear optical responses.

H. Weng, *Nat. Mat*. **18**, 428 (2019).

Floquet engineering of interlayer couplings in twisted bilayers: graphene and $MoTe_2$

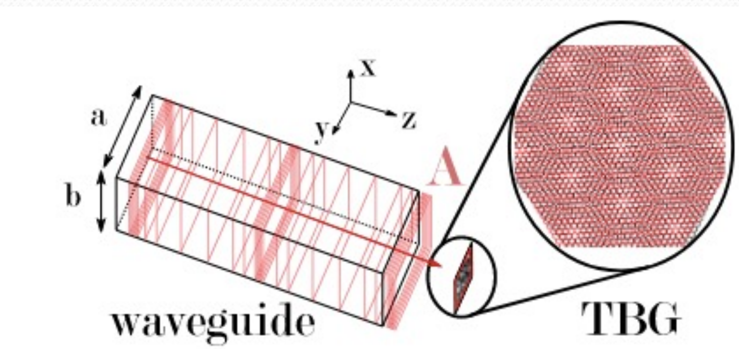

$$T_n = w_0 \mathbb{1}_2 + w_1 \left[\cos\left(\frac{2\pi n}{3}\right)\sigma_1 + \sin\left(\frac{2\pi n}{3}\right)\sigma_2 \right]$$

$$w_1 \to w_1 e^{-i a_{AB} A \cos(\Omega t)}$$

$$w_0 \to w_0 e^{-i a_{AA} A \cos(\Omega t)}$$

Magic angles:

$$\theta_n = \frac{w_1 J_0(|a_{AB} A|)}{v_F k_D \alpha_n}$$

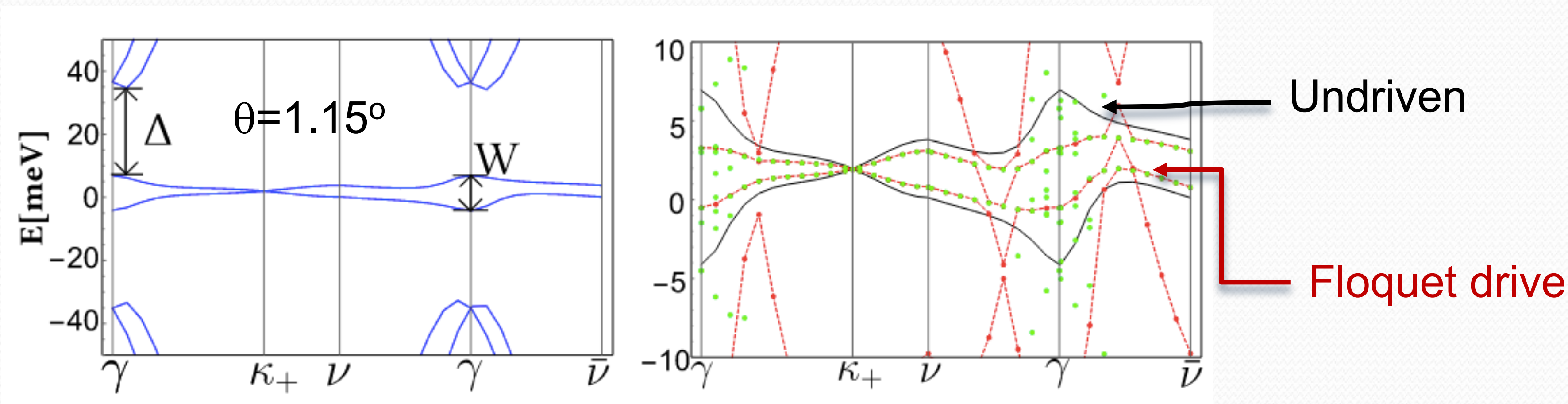

M. Vogl, M. Rodriguez-Vega, and GAF *Phys. Rev. B* **101**, 241408(R) (2020).
M. Vogl, M. Rodriguez-Vega, B. Flebus, A. H. MacDonald, and GAF *Phys. Rev. B* **103**, 014310 (2021). [$MoTe_2$—Topological band transitions at the end of waveguide.]

Simultaneous excitation of phonons *and* electrons in bilayer graphene

Adopt an atomically adiabatic model: V. Mohanty and E. J. Heller, *PNAS* **116**, 18316 (2019).

$$\mathcal{H} = -\sum_{\boldsymbol{R}}\sum_{n=1}^{3}\gamma_0(\boldsymbol{\delta}_{n,1}^2)a_1^\dagger(\boldsymbol{R})b_1(\boldsymbol{R}+\boldsymbol{\delta}_{n,1}) - \sum_{\boldsymbol{R}}\sum_{n=1}^{3}\gamma_0(\boldsymbol{\delta}_{n,2}^2)b_2^\dagger(\boldsymbol{R})a_2(\boldsymbol{R}+\boldsymbol{\delta}_{n,2}) - \gamma_3\sum_{\boldsymbol{R}}a_1^\dagger(\boldsymbol{R})b_2(\boldsymbol{R}+\boldsymbol{\delta}_{n,1}) - \gamma_1\sum_{\boldsymbol{R}}a_2^\dagger(\boldsymbol{R})b_1(\boldsymbol{R}) + \text{H.c.},$$

$$\gamma_0(\delta^2) = c_1 e^{-c_2\delta^2}$$

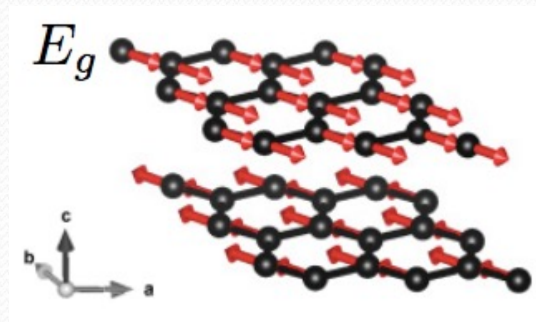

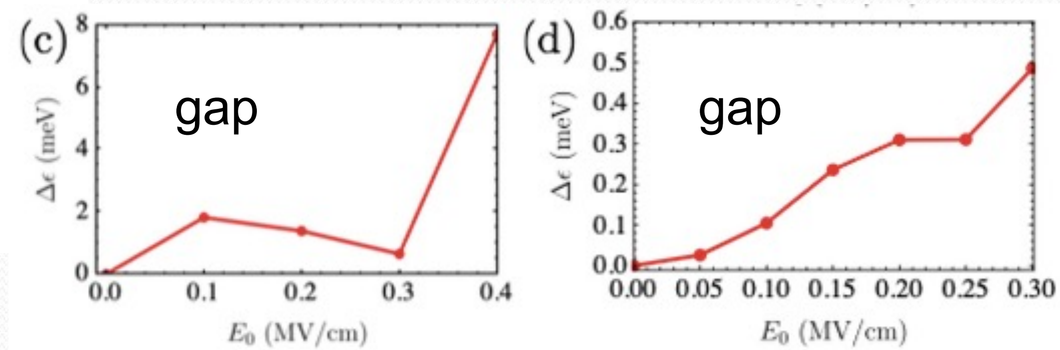

Phonons+electrons

Phonon only

M. Vogl, M. Rodriguez-Vega, and GAF *Phys. Rev. B* **104**, 245135 (2021).

AF insulators with tunable magnon-polaron Chern numbers (non-driven phonons)

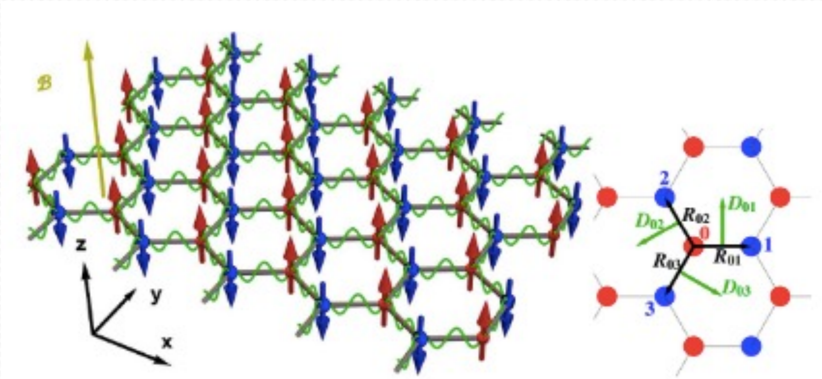

In-plane optical phonons couple to magnetization.

Mirror-symmetry breaking allows in-plane DM.

$$H = H_m + H_p + H_{mp}$$

$$H_p = \sum_i \frac{\mathbf{p}_i^2}{2M_i} + \frac{k_1}{2}\sum_{\langle ij\rangle}(\hat{\mathbf{R}}_{ij}^0 \cdot \mathbf{u}_{ij})^2 + \frac{k_2}{2}\sum_{\langle\langle ij\rangle\rangle}(\hat{\mathbf{R}}_{ij}^0 \cdot \mathbf{u}_{ij})^2$$

$$H_m = J_1 \sum_{\langle ij\rangle} \mathbf{S}_i \cdot \mathbf{S}_j - J_2 \sum_{\langle\langle ij\rangle\rangle} \mathbf{S}_i \cdot \mathbf{S}_j - \frac{K_z}{2}\sum_i (S_i^z)^2 - \mathcal{B}\sum_i S_i^z,$$

External B-field tunes magnon-polaron Chern numbers

$$H_{mp} \approx \frac{DS}{a}\sum_{\langle ij\rangle} \mathbf{u}_{ij}[\mathcal{I}_2 - \hat{\mathbf{R}}_{ij}^0\hat{\mathbf{R}}_{ij}^0](\delta\mathbf{s}_{A,i} + \delta\mathbf{s}_{B,j}) = \frac{DS}{a}\sum_{\langle ij\rangle}(\hat{\mathbf{R}}_{ij}^0 \times \mathbf{u}_{ij}) \cdot [\hat{\mathbf{R}}_{ij}^0 \times (\mathbf{S}_{A,i} + \mathbf{S}_{B,j})]$$

$$H_D = \mathbf{D}_{ij} \cdot (\mathbf{S}_i \times \mathbf{S}_j)$$

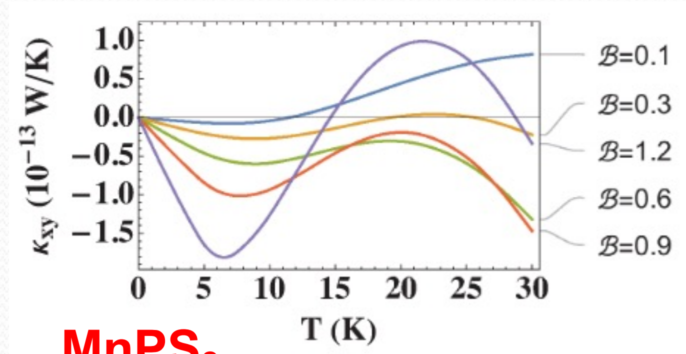

(a)

$MnPS_3$

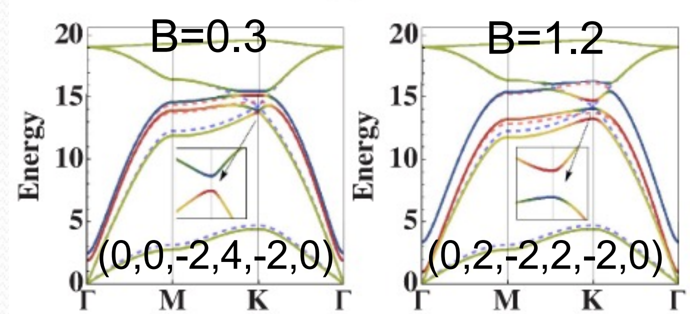

(b) (c)

B. Ma and GAF, *Phys. Rev. B*. **105**, L100402 (2022).